Higher-order epistasis within Pol II trigger loop haplotypes

Authors: Bingbing Duan[1], Chenxi Qiu[2], Steve W. Lockless[3], Sing-Hoi Sze[4,5], Craig D. Kaplan[1*]

Affiliations:

[1] Department of Biological Sciences, University of Pittsburgh, Pittsburgh, PA 15260.

[2] Department of Genetics, Harvard Medical School, Boston, MA 02215.

[3] Department of Biology, Texas A&M University, College Station, TX 77843.

[4] Department of Computer Science & Engineering, Texas A&M University, College Station, TX 77843.

[5] Department of Biochemistry & Biophysics, Texas A&M University, College Station, TX 77843.

Contact information: craig.kaplan@pitt.edu

ABSTRACT

RNA polymerase II (Pol II) has a highly conserved domain, the trigger loop (TL), that controls transcription fidelity and speed. We previously probed pairwise genetic interactions between residues within and surrounding the TL and identified widespread incompatibility between TLs of different species when placed in the *Saccharomyces cerevisiae* Pol II context, indicating epistasis between the TL and its surrounding context. We sought to understand the nature of this incompatibility and probe higher order epistasis internal to the TL. We have employed deep mutational scanning with selected natural TL variants ("haplotypes"), and all possible intermediate substitution combinations between them and the yeast Pol II TL. We identified both positive and negative higher-order residue interactions within example TL haplotypes. Intricate higher-order epistasis formed by TL residues was sometimes only apparent from analysis of intermediate genotypes, emphasizing complexity of epistatic interactions. Furthermore, we distinguished TL substitutions with distinct classes of epistatic patterns, suggesting specific TL residues that potentially influence TL evolution. Our examples of complex residue interactions suggest possible pathways for epistasis to facilitate Pol II evolution.

INTRODUCTION

Functional interactions among amino acid residues within a protein can be detected by genetic interactions in the form of epistasis. Epistasis can determine the phenotypic effects of mutations. Specific substitutions can constrain or relax functional constraints on the identity of residues at other positions, and impact evolutionary trajectories (MANI *et al.* 2008; PHILLIPS 2008; STARR AND THORNTON 2016; DOMINGO *et al.* 2019; PARK *et al.* 2022; JOHNSON *et al.* 2023; METZGER *et al.* 2023). Epistasis is the modulation, positive or negative, of the effect of one mutant by the presence of other mutants. Phenotypic modulation of one mutant by another (epistasis) can be detected by a difference in the phenotype of a double mutant from that expected from the cumulative effects of the corresponding single mutants, which is the baseline expectation in the absence of epistasis (PHILLIPS 1998; HILL *et al.* 2008; MANI *et al.* 2008; PHILLIPS 2008). Prior studies found many epistatic interactions at both lower-orders (i.e. among residue pairs) and higher-orders (among many residue combinations). Higher-order epistasis emerging from particular residues can reflect specific biological or physical interactions and imply crucial roles of these residues in a protein's function and evolution (MELAMED *et al.* 2013; OLSON *et al.* 2014; BANK *et al.* 2015; POKUSAEVA *et al.* 2019; REDDY AND DESAI 2021; BAKERLEE *et al.* 2022; DING *et al.* 2022; LIN *et al.* 2022). In this work, we dissect complex higher-order epistasis by deep mutational scanning within an ultra-conserved and crucial active site domain, the trigger loop (TL), of RNA polymerase II (Pol II).

Pol II transcribes eukaryotic mRNA using an iterative nucleotide addition cycle (NAC) (BAR-NAHUM *et al.* 2005; WANG *et al.* 2006; MALINEN *et al.* 2012; DANGKULWANICH *et al.* 2013; KAPLAN 2013). The TL is a critical domain for the NAC, and participates in all three steps: nucleotide selection, catalysis, and likely translocation by switching between different conformations (WANG *et al.* 2006; FOUQUEAU *et al.* 2013; BARNES *et al.* 2015). In each NAC, a matched substrate entering the active site induces or captures a conformational change of the TL from an open, catalysis-disfavoring state to a closed, catalysis-favoring state. Thus, the TL functions in kinetic selection to distinguish matched NTPs complementary to the DNA template from mismatched ones (WANG *et al.* 2006; HUANG *et al.* 2010; MALINEN *et al.* 2012; KAPLAN 2013; WANG *et al.* 2013; XU *et al.* 2014; BARNES *et al.* 2015). Full closure of the TL promotes catalysis (VASSYLYEV *et al.* 2007; WANG *et al.* 2013). Following catalysis, the TL transits from the closed to the open state, facilitating polymerase translocation for the subsequent NAC (SEIBOLD *et al.* 2010; DA *et al.* 2012; LIU *et al.* 2016)(**Fig. 1A**). Additional TL confirmations have been

associated with other RNA polymerase activities such as pausing and backtracking (WANG *et al.* 2009; ZHANG *et al.* 2010; CHEUNG AND CRAMER 2011; MOSAEI AND ZENKIN 2021). With these transitions, the mobile TL balances transcription fidelity and speed (WANG *et al.* 2006; KAPLAN *et al.* 2008; KIREEVA *et al.* 2008; SYDOW *et al.* 2009; KAPLAN 2010; YUZENKOVA *et al.* 2010; LARSON *et al.* 2012; UNARTA *et al.* 2023). How do residues within the TL interact with each other to ensure its proper transition? Our observations of distinct pairwise interactions suggest that TL function is maintained by residue interaction networks (DUAN *et al.* 2023). For example, previous biochemical and genetics studies found mutations in the TL can modify its folding or dynamics, causing changes in catalytic activity - either an increase, leading to faster elongation rate than WT in vitro (gain of function, GOF) or a decrease, leading to slower elongation rate than WT in vitro (loss of function, LOF) (KAPLAN *et al.* 2008; KIREEVA *et al.* 2008; KAPLAN *et al.* 2012; BRABERG *et al.* 2013; NAYAK *et al.* 2013; WINDGASSEN *et al.* 2014; BARNES *et al.* 2015; QIU *et al.* 2016). With TL double mutants including combinations between or within GOF and LOF mutations, our prior work identified distinct types of pairwise interactions resulting in either better than expected fitness from the cumulative model, i.e. suppression, commonly observed in GOF/LOF combinations, or worse than expected, i.e. synthetic sickness or lethality, normally seen in combinations of the same class (GOF/GOF or LOF/LOF). These interactions are consistent with a model that the involved single mutants independently act within double mutants, where effects are balanced in double mutants comprising constituent mutants with opposite effects and effects are enhanced in double mutants comprising constituent mutants with similar effects (KAPLAN *et al.* 2012; QIU *et al.* 2016; QIU AND KAPLAN 2019; DUAN *et al.* 2023). However, we also observed both lack of enhancement for some “same class” combinations (epistasis), and cases where a mutant’s effect appeared to be controlled by the identity of another residue (sign epistasis) (KAPLAN *et al.* 2012; QIU *et al.* 2016; QIU AND KAPLAN 2019; DUAN *et al.* 2023).

The TL is highly conserved across evolution, supporting the idea that identities of key residues are highly constrained (PALO *et al.* 2021). Given this conservation, it was surprising that analogous mutations in a highly conserved residue yielded opposite effects in the conserved yeast Pol I and Pol II (VIKTOROVSKAYA *et al.* 2013). Given the TL’s flexible and mobile character, and its high conservation of sequence and function, it was an open question of how self-contained it is functionally and if there is evolutionary coupling through non-conserved residues to maintain its ability to achieve its different conformations. Our recent studies identified widespread incompatibility between trigger loops of different species or enzymes placed into the yeast Pol II context, supporting the idea of an epistasis network from residues outside the TL is prominent in constraining TL function across evolution (DUAN *et al.* 2023). We wished to understand the drivers of this incompatibility between conserved TLs and use diverse TL haplotypes to probe the complexity of internal TL interactions.

Recent studies have suggested that the primary contributor of epistasis to protein function is through pairwise residue interactions. Higher order epistasis is complicated and can be difficult to detect (JOHNSON *et al.* 2023; METZGER *et al.* 2023). We reasoned that the Pol II TL might be an excellent system to detect higher order epistasis using evolutionary haplotypes, notwithstanding constraints on function from the rest of the enzyme complex. The Pol II TL is flexible, being required to support distinct conformational states, and functionally plastic in that mutants can both increase or decrease catalysis with known suppressor relationships between these two types of mutants. We applied our TL deep mutational scanning system to detect higher order epistasis by comprehensive dissection of a set of evolutionarily derived TL sequences (haplotypes). We identified intra-TL interactions of evolutionarily observed substitutions (TL-internal epistasis) and dissected specific examples of complex interactions that would not be evident from simple analyses only considering single mutants or complete

haplotypes. Our experiments suggest specific paths for TL evolution in the context of the complete enzyme may likely go through mild gain-of-function residues that allow additional changes to be tolerated.

RESULTS

Systematic detection of epistatic interactions within TL haplotypes. We utilized our previously developed deep mutational scanning-based phenotyping platform for Pol II mutants in *Saccharomyces cerevisiae* (QIU *et al.* 2016; DUAN *et al.* 2023) to analyze TL-internal higher-order epistasis. The analyzed TL haplotypes included 662 natural TL variants from bacterial and archaeal msRNAPs, and eukaryotic Pol I, Pol II and Pol III (**Fig. 1B-C**). An additional 1987 TL alleles were included, representing all possible intermediate substitution combinations for seven selected natural Pol II TL variants (**Fig. 1D**). The seven TL variants were selected because they contain specific amino acids which exhibit phenotypes, either GOF or LOF, when introduced individually in yeast Pol II. The functional consequences of these haplotypes were measured by a set of growth phenotypes that are predictive of biochemical functions (see **Methods**)(KAPLAN *et al.* 2012; QIU *et al.* 2016; QIU AND KAPLAN 2019; DUAN *et al.* 2023). Our system allows us to profile these haplotypes and assess epistasis among multiple mutations in a highly parallel fashion.

To detect epistasis, we first fitted a log additive model for the fitness of individual mutations, which assumes all the individual mutations are independent and additive (HILL *et al.* 2008; MANI *et al.* 2008; PHILLIPS 2008; LIN *et al.* 2022; DUAN *et al.* 2023) and we then computed how the observed fitness of haplotypes deviates from the predicted fitness by the log additive model. Here fitness is determined by comparing the allele frequency shifts of a mutant under selective conditions relative to control conditions, and then comparing the allele frequency change of mutants to the change observed in the WT (see **Methods**). The log of the fitness is defined as a fitness score. The log additive model assumes individual mutations are independent, so the fitness effects of individual mutations are multiplied in the double/multiple mutants (the log of the fitness scores are additive). Deviation from the log additive model is evidence for residue interactions (epistasis). Deviation from expectation could be in the form of mutual suppression (double mutant more fit than either single mutant), basic epistasis (double mutant no worse than one of the single mutants), or synthetic sickness (greater than log additive defects in the double mutant). The deviation values, termed “deviation scores”, were calculated to detect intra-TL genetic interactions within haplotypes (see **Methods**).

Deviation scores were calculated in two ways. We determined a “primary deviation” score, representing total epistasis within a haplotype as the deviation of the predicted fitness from the sum of the fitness scores of individual mutants (**Fig. 1E and Fig. S1**). Second, to determine which residues the epistasis emerged from, we separated the haplotypes into combinations of single substitutions plus the compound mutant formed by the remaining substitutions. We therefore calculated a secondary deviation score by comparing the fitness score of the complete haplotype to the sum of the single substitution’s fitness score and the fitness score of the compound consist of the remaining substitutions (**Fig. 1F and Fig. S1**). The magnitude of the secondary deviation score indicates the magnitude of epistatic effects for specific substitutions when they are introduced to the compound mutant. Moreover, analyzing the secondary deviation scores of a specific substitution across various compound mutants (backgrounds) enables us to assess the breadth of its epistatic effects, which may reveal its potential to impact TL evolution.

Drivers of incompatibility for TL variants placed in the yeast Pol II context. We explored potential reasons for the widespread incompatibility between TL haplotypes from other msRNAPs and yeast Pol II (VIKTOROVSKAYA *et al.* 2013; QIU *et al.* 2016; DUAN *et al.* 2023). To probe this incompatibility, we grouped haplotypes based on their evolutionary source (Bacteria, Archaea and eukaryotic Pol I, Pol II and Pol III) and illustrated the fitness of all constituent single substitutions measured in yeast Pol II (QIU *et al.* 2016; DUAN *et al.* 2023), the expected fitness of the haplotypes calculated based on the log additive model, the observed fitness of the haplotypes measured from our deep mutational scanning, and the primary deviation score from comparison of the observed and expected fitness (**Fig. 2A-E**). The incompatibility of Bacterial TLs in yeast was explained by the presence of three substitutions that are individually lethal in yeast (**Fig. 2A**). Interestingly, among archaeal TLs examined, only about half could be explained by individual lethal substitutions while others appeared lethal due to simple additivity of mutant phenotypes. A subset however appeared to illustrate negative epistasis among constituent substitutions (**Fig. 2B**). Fewer individually lethal single substitutions were observed in eukaryotic Pol I, Pol III and Pol II haplotypes than those in Bacteria and Archaea, while more positive or negative intra-TL interactions appeared (**Fig. 2C-G**), likely due to eukaryotic Pols being closer to Pol II in evolution. Surprisingly, a few single substitutions from other Pol II TL haplotypes were lethal in yeast Pol II context (**Fig. 2D**), indicating that even in highly conserved Pol II enzymes, epistasis between the TL and its Pol II context is specific and important functional constraints have evolved among close homologs.

We then asked if functional coupling of residue identities within the TL across evolution might correlate with positive interactions (**Fig S2A-C**). This analysis tests the hypothesis that internal coupling of residues within the TL could be important for its function even outside of their coevolved, appropriate contexts. Statistical coupling analysis is a powerful approach to identify functional interactions by statistical inference of residue identities that appear to correlate across evolution (RUSS *et al.* 2005; SOCOLICH *et al.* 2005). We detected 11 residues involved in coupling within the TL domain using a multiple sequence alignment containing 362 eukaryotic TL sequences (natural TL variants) (**Fig. S2A**). To test if statistical coupling within the TL is implicated in TL function and detectable for TL haplotypes removed from their natural context, we designed two libraries to perturb residue coupling in large scale, as previously described (RUSS *et al.* 2005; SOCOLICH *et al.* 2005). One library comprised scrambled haplotypes that retained TL-internal residue couplings and conservation as determined from natural TL variants (“Monte Carlo” scrambling library) (**Fig. S2C**). A second library comprised scrambled haplotypes but only preserved conservation but not any TL-internal residue coupling (“Random scramble” library) (See **Methods**) (**Fig. S2B**). Both libraries satisfy the design parameters as indicated by residue distributions (**Fig S2A-C**). If substantial internal TL epistasis were present within the evolutionary signal, we would predict that haplotypes in the Monte Carlo scramble library would have greater fitness on average than those from Random scramble library. We did observe more Monte Carlo scrambled haplotypes in the viable range (fitness from -6.0 to 0) than the random scramble; conversely, more random scrambled haplotypes were in the severe sick/lethal range (fitness around -6.5). The difference was subtle but significant (P-value = 0.006), suggesting that without positive epistasis between TL alleles and their appropriate coevolved contexts, TL-internal epistasis is weak or undetectable based on our tested couplings.

Epistasis within TL haplotypes can be attributed to residues. We next determined from which residues the epistatic effects in TL haplotypes emerge. We selected seven Pol II TL

variants based on their diversity where each have 7~9 substitutions relative to the *S. cerevisiae* Pol II TL, and we constructed 1987 unique intermediate haplotypes representing 2169 combinations of substitutions from the seven variants. These seven variants cover a range of compatibility with yeast Pol II function as determined by their fitness when replacing the yeast Pol II TL (**Fig. 3A-H)**. Four out of seven TL variants were not compatible in the yeast Pol II context for distinct reasons. The TL variant from *G. luxurians* was lethal presumably because it encodes G1088S, which causes lethality on its own and was similarly deleterious for all intermediate genotypes (**Fig. 3A, C**). In contrast, lethalities of TL variants from *B. anathema* and *R. solani* were not explained by presence of an individual lethal substitution, and they were predicted to be viable by the summation of the fitness scores of individual substitutions. These observations suggested that the observed lethality for these two haplotypes is due to negative interactions among residues (lethality beyond additivity) (**Fig. 3A, G, H**). The *S. rosetta* TL was both expected and observed to be lethal, supporting lethality from additivity of residues (**Fig. 3A).** However, it's worth noting that *S. rosetta* intermediate combinations with specific substitutions exhibited fitness in the lethal range **(Fig. 3F**) but were worse than predicted from the log additive model, suggesting negative interactions. In three out of seven variants, where all individual substitutions were viable and combinations between them were predicted to be viable based on the log additive model, some intermediate substitution combinations were in the severely sick or lethal range (**Fig. 3B, D, E and S3**), implying negative interactions among the substitutions. Interestingly, this lethality of intermediate genotypes was suppressed by additional substitutions, resulting in final viable haplotypes and indicating positive interactions (**Fig. 3B, D, E**). The fluctuations of the fitness with various residue combinations suggests complexity and potential higher order epistasis within these TL haplotypes.

To determine which specific residues contribute to the observed epistasis, we assessed deviation from expected fitness for the addition of each substitution to all intermediate haplotypes derived from subsets of substitutions of the haplotype. This analysis allows mutant effects to be compared for multiple related backgrounds (the intermediate states representing subsets of haplotype substitutions) (**Fig. 1D, F**). The fitness and epistatic effects of each substitution are shown as epistasis heatmaps (**Fig. 4 and S4**). For example, we observed better fitness for the *E. invadens IP1* TL haplotype than predicted from the log additive model (**Fig. 4A**), suggesting positive interaction(s) within the eight substitutions comprising the haplotype. Among these eight are two with biochemically classifiable phenotypic profiles as determined from library screening of single substitution mutants on conditional media – the LOF variant V1089T and the GOF variant S1096E. Consistent with these alleles being candidates for epistatic effects, these two substitutions also have the lowest relative growth fitness of the eight *E. invadens IP1* TL substitutions (**Fig. 4A-B**). S1096E had positive secondary deviation scores in most intermediate combinations, suggesting broad effects. V1089S showed positive effects but mostly in intermediates that also contained S1096E (**Fig. 4B**), suggesting that V1089S's positive effect was dependent on S1096E, likely due to the suppression predicted from the combination of GOF and LOF substitutions. Interestingly, S1091E, a substitution without strong growth fitness and with no obvious phenotypes as a single substitution, showed strong positive or negative epistatic effects in most backgrounds (**Fig. 4B**). These results suggest these three substitutions are responsible for intra-TL epistasis within *E. invadens IP1* TL haplotype.

To visualize these effects, we quantified the impact of constituent substitutions on epistasis within the haplotype by identifying correlations between the primary deviation score, which represents the overall epistasis of the haplotype, and the secondary deviation scores, which

represents the specific epistatic effects of individual substitutions on corresponding haplotype backgrounds. Substitutions with stronger correlation (higher linear regression R^2) indicate these substitutions are the main drivers of the epistatic effects observed for the entire haplotype. Conversely, substitutions with low correlation (smaller R^2) suggest that the respective substitutions have no specific, or limited contributions to epistasis within the haplotype. To demonstrate this concept, we created a simplified simulation (**Fig. S4**). Consider a TL haplotype comprising five substitutions: a, b, c, d, and e. In this scenario, the single mutant “a” is GOF, “b” and “c” are LOF, whereas “d” and “e” have no effects. We set the suppression interactions in GOF+ LOF combinations (a/b and a/c), and synthetic sick interactions in the LOF+ LOF combination b/c (**Fig. S4A**). We calculated all primary and secondary deviation scores for the haplotype and all intermediate combinations. The GOF mutant “a” exhibited positive secondary deviation scores in most intermediates (**Fig. S4B**). The secondary deviation scores of three single mutants with phenotypes showed strong correlation (R^2) with the primary deviation scores (**Fig. S4C**), showing they are the key contributors to the observed epistatic interactions within haplotypes. The correlations observed between secondary deviation scores of “a” versus “b” and “c” indicate the secondary deviation scores of “b” and “c” are positive in most cases when “a” is present (**Fig. S4D**), suggesting “b” and “c” potentially suppresses "a”. Similarly, the secondary deviation scores of “a” are consistently positive with changes in secondary deviation scores of “b” (**Fig. S4E**) and “c” (**Fig. S4F**), indicating “a” suppresses “b” and “c”. These observations confirmed the mutual suppression in GOF and LOF combinations. Conversely, LOF substitutions “b” and “c” showed correlated secondary deviation scores, showing their synthetic sick interactions.

To detect the key contributors to epistatic interactions observed in the *E. invadens IP1* TL haplotype, we determined the correlations between the primary and secondary deviation scores. Consistent with the epistasis landscape (**Fig. 4B**), the secondary deviation scores of S1096E, V1089T, and S1091E have strong correlations ($R^2 > 0.5$) with the primary deviation score (**Fig. 5A**), suggesting their substantial effect on the primary epistasis of the haplotype. ~1-3 substitutions with notable effects on haplotype epistasis were identified for all seven selected TL variants (**Fig 4B, 5A, and Fig. S5-S6**), suggesting epistasis within haplotypes is attributable to subsets of substitutions.

The epistasis within TL haplotypes can reflect intricate residue interactions. We dissected the interactions formed by the three substitutions S1096E, V1089T, and S1091E in the *E. invadens IP1* TL haplotype and observed an intricate, higher-order epistasis network (**Fig. 5A-G**). First, we confirmed the mutual suppression between the GOF S1096E and the LOF V1089S. S1096E had a consistent positive epistatic effect in haplotypes containing V1089T **(Fig. 5B**). V1089T exhibited a smaller but similar positive effect on haplotypes containing S1096E (**Fig. 5C**), illustrating mutual suppression between V1089T and S1096E. These observations are consistent with the predicted suppression between GOF and LOF mutants and is illustrated by the positive values for their combinations shown in **Fig. 4B**. Additionally, we observed negative interactions for S1091E when it was combined with F1086H/V1089T/K1093T, but these were dependent on the absence of S1096E. This was indicated by a low secondary deviation for S1091E when S1096E was present (**Fig. 5C-D**)**.** These observations are interpreted as S1096E being epistatic to S1091E. We identified negative interactions in six intermediate combinations containing S1091E, as suggested by their fitness in the ultra-sick or lethal range beyond the log additive model (**Fig. 5E**). Strikingly, F1086H, V1089T, K1093T were present in all six intermediate combinations with S1091E, pointing to negative synergistic interaction (synthetic

sickness or lethality) between the four substitutions. Conversely, S1096E was absent in all six combinations (**Fig. 5E**), implying the negative interaction may be suppressed by S1096E. We confirmed the suppression by the observation that the fitness of all six ultra-sick/lethal combinations with S1096E incorporated was out of the ultra-sick/lethal range (fitness > -5) (**Fig. 5F**) and by spot assay (**Fig. S7**). We summarize all the observed interactions in **Fig. 5G**, representing the complicated higher-order epistasis network.

Substitutions of the *P. persalinus (Ciliate)* TL haplotype formed two higher-order epistasis networks. The complexity of these epistasis networks arises from the intricate layers of substitution interactions. Notably, these interactions were not immediately apparent when observing all substitutions in the entire haplotype, meaning that the predicted and expected fitnesses for the complete haplotype were similar (**Fig. 6 and Fig. S8-S9**). First, the haplotype contains nine single substitutions with no or slight growth fitness defects. The observed fitness of the haplotype was very similar to expected from the log additive of all individual substitutions' fitnesses, with the calculated primary deviation score close to 0. Second, when we dissected potential interactions in substitution combinations, we noticed two substitutions exhibited distinct behavious, A1076T and V1089S. Since both of these residues are classifiable as having predicted biochemical phenotypes (A1076T as a GOF and V1089S as a LOF), we anticipated suppression between them and predicted they would be drivers of epistatic interactions within intermediate combinations. Consistently, suppression was observed when A1076T and V1089S were combined (**Fig. S8**), and the correlations between the secondary and primary deviation scores suggest that A1076T and V1089S strongly affect the epistasis in the haplotypes (**Fig. 6B**). Additionally, two intermediate combinations, each with five substitutions, appeared to have the lowest primary and secondary deviation scores (the labeled **I** and **II in Fig. 6B**), implying negative interactions (synthetic sickness/lethality) within the two combinations respectively. The combination I, A1076T/A1090S/S1091D/S1096L/I1104L, showed a negative primary deviation score (observed fitness < expected fitness) (**Fig. 6C**), illustrating synthetic sickness among the five substitutions. The secondary deviation scores of five constituent substitutions were all negative (**Fig. 6C**), implying the synthetic sickness could be attributed to addition of each substitution to a combination of the others. The remaining four substitutions, V1089S, K1092R, K1093N, and K1102Q all showed positive secondary deviation scores when they are incorporated into the combination, suggesting each one of them could individually suppress the synthetic sick combination (**Fig. 6C**). The observed interaction network is shown in **Fig. 6D**. In contrast, sign epistasis was observed in the combination II, A1076T/A1090S/S1091D/K1092R/K1093N, where the GOF sign of A1076T appeared to change to LOF when A1090S/S1091D/K1092R/K1093N were present simultaneously with A1076T. In detail, the combination has a negative primary deviation score, representing negative interaction among the substitutions (**Fig. 6E**). Surprisingly, the negative interaction only appeared when the four substitutions, A1090S, S1091D, K1092R, and K1093N were present simultaneously with A1076T (**Fig. S9A**), and there were no obvious interactions among the four substitutions (**Fig. S8**), suggesting the interaction between A1076T and the combination of the four substitutions A1090S/S1091D/K1092R/K1093N. We infer a change from GOF to LOF for A1076T due to the observation of lethality upon incorporation of LOF V1089S into the combination. While A1076T *suppresses* V1089S in backgrounds in nearly all synthetic sick/lethal combinations between V1089S and individual substitutions or intermediate combinations of A1090S, S1091D, K1092R, and K1093N, it *enhances* the growth defect of V1089S/A1090S/S1091D/K1092R/K1093N. This outcome aligns with the expectation of lethality

in a combination with the same class substitutions (LOF V1089S and the LOF A1076T). (**Fig. S9B-C**). These observations are consistent with the combination of A1090S/S1091D/K1092R/K1093N converting A1076T from a GOF to a LOF. Notably, S1096L, K1102Q, and I1104L could individually suppress A1076T/A1090S/S1091D/K1092R/K1093N when they were incorporated into the combination, as indicated by their positive secondary deviation scores (**Fig. 6E**), implying each one of them could revert the sign epistasis within A1076T/A1090S/S1091D/K1092R/K1093N. V1089S is now suppressible by A1076T when either S1096L, K1102Q, or I1104L are present (**Fig. 6F**). In summary, these higher order interaction networks observed in the *P. persalinus (Ciliate)* TL haplotype (**Fig. 6E-F**) emphasize the complexity of higher-order epistasis, revealing layers of interactions beneath the surface.

Distinct categories of residue epistasis patterns. To comprehensively compare the magnitude and consistency of epistatic effects of TL substitutions when introduced into different genetic backgrounds, we determined the distributions of secondary deviation scores for each substitution. Substitutions with strong epistatic effect (**Fig. 4 and S5**) and primary/secondary score correlations (**Fig. 5A, Fig. 6B, and Fig. S6**), display wide distributions of secondary deviation scores. Interestingly, while most of these impactful substitutions have classifiable phenotypes as single substitutions (GOF or LOF) (**Fig. S10A-F**), some without obvious phenotypes still show wide ranges of epistatic impacts, such as S1091E (**Fig. S10A**), K1093N (**Fig. S10E-F**), A1076G and N1082K (**Fig. S10G**). Notably, some substitutions, like A1076T, were present in more than one TL haplotype background (**Fig. S10C-F**). To evaluate the overall epistatic effects of these substitutions in all tested backgrounds, we displayed the density plots of their secondary deviation scores across all non-repetitive haplotypes in which they are found (**Fig. S11**) and calculated the maximum likelihood estimate (σ^2) to quantify the distribution of secondary deviation effect for each substitution (PARK *et al.* 2022) (**Fig. 7A**). 62.5% of substitutions exhibit mild epistatic effects ($\sigma^2 < 3$) and 25% of substitutions have medium effect ($3 \leq \sigma 2 \leq 5$). A small portion, 12.5% of substitutions, show strong epistatic effects ($\sigma^2 > 5$). The epistatic effects of substitutions did not correlate with their fitness as single substitutions (**Fig. S12A**). Moreover, the distribution of a substitution's secondary deviation scores is expected to follow normal distribution if the substitution has no or minor epistatic effect in backgrounds to which it is introduced (PARK *et al.* 2022). However, ~80% of TL substitutions did not have normally distributed secondary deviation scores (**Fig. S12B**), illustrating that most TL substitutions had epistatic effects when introduced into some if not all genetic backgrounds. To investigate whether the epistatic effects of substitutions consistently remained positive (or negative) across various genetic backgrounds, we calculated the median of secondary deviation scores for substitutions respectively and plotted them against the corresponding σ^2 values. Substitutions with strong epistatic effects (σ^2) exhibited higher positive (or negative) median values (**Fig. 7B**), implying that substitutions with robust epistatic effects consistently displayed either positive or negative impacts across various genetic backgrounds. We further compared the epistatic effects of substitutions in three categories (**Fig. 7C**). Substitutions with a mild epistatic effect had little impact on the fitness of haplotypes when introduced. Substitutions with a medium epistatic effect, like A1076T and K1093N, could either enhance or reduce fitness of haplotypes. In contrast, substitutions with strong epistatic effects, such as S1096E and R1100C, were epistatic to backgrounds where they were observed, consistent with their requirement for toleration of specific substitutions in those backgrounds.

DISCUSSION

RNA polymerase TL function and evolution is impacted by extensive residue interactions within and around it (KAPLAN *et al.* 2012; DUAN *et al.* 2023). The TL shows remarkable conservation consistent with its essential tasks for executing mechanisms in all msRNAPs (CRAMER 2002; WERNER AND GROHMANN 2011; BELOGUROV AND ARTSIMOVITCH 2019; MAZUMDER *et al.* 2020). Our observation (DUAN *et al.* 2023) of widespread TL incompatibility in the *S. cerevisiae* Pol II context suggested epistasis external to the TL is the major source of epistasis for TL function (**Fig. S2**). However, here we observed TL-internal epistatic interactions and residue coupling, although TL-internal coupling did not significantly maintain TL function when the interaction between TL and its greater evolutionary context was broken. The analyses in our recent work (DUAN *et al.* 2023) and here indicate interactions formed by TL residues are integrated into the broader residue epistasis network within the whole enzyme (**Fig. 2**). In summary, our results are in line with observations from other studies where the same mutation led to different phenotypes when introduced into homologous proteins (KONDRASHOV *et al.* 2002; LUNZER *et al.* 2010; NATARAJAN *et al.* 2013; VIKTOROVSKAYA *et al.* 2013; DOUD *et al.* 2015; STARR AND THORNTON 2016; HADDOX *et al.* 2018; PARK *et al.* 2022), highlighting the divergent nature of epistasis networks in highly conserved proteins like msRNAPs.

Even considering our above findings, our experiments here provide case studies for examples of complex interactions during evolutionary divergence. The divergence in epistasis networks of homologs accumulates through substitutions. How substitutions alter existing epistasis and shape the effects of future substitutions is critical for understanding mechanisms underlying protein functional divergence and evolution (STARR AND THORNTON 2016; JOHNSON *et al.* 2023; XIE *et al.* 2023). Using seven selected Pol II TL variants, we comprehensively determined the higher-order epistatic interactions these substitutions create. For example, S1096E exhibited strong suppression on all synthetic sick/lethal combinations of *E. invadens IP1* TL haplotype substitutions (**Fig. 5 and S7**), suggesting a potential path for TL evolution that would require the 1096E substitution prior to additional substitutions that lead to synthetic sickness/lethality. A caveat to this interpretation is that additional substitutions outside the TL might reshape epistasis across the entire TL. Additionally, A1076T, a substitution that consistently showed positive epistatic effects when introduced into different genetic backgrounds (**Fig. 7C**), was also subject to sign epistasis in certain backgrounds. Here, we would propose that additional substitutions that prevent this sign epistasis might precede appearance of a combination that would otherwise incur a fitness defect with A1076T (**Fig. 6E-F**). A1076T-involved sign epistasis exemplifies intricate layers of substitution interactions. Emerging substitutions modify pre-existing interactions, ultimately influencing the fate of future mutations and the trajectory of protein evolution.

We further inquired whether all individual substitutions had the potential to change the pre-existing epistasis networks in the protein background they were introduced into, and to what extent. To investigate this, we analyzed the strength and consistency of the epistatic effects of substitutions across diverse genetic backgrounds. The epistatic effects of TL substitutions can be categorized into three distinct groups, with approximately 37.5% of TL substitutions consistently demonstrating medium to strong and stable epistatic effects, either positive or negative (**Fig. 7A-B**), reflecting their important role in reshaping the interactions among fixed historical substitutions and influencing the phenotypes of upcoming mutations. Substitutions that consistently exhibit positive epistatic effects, such as A1076T and S1096E (**Fig. 7C**), are referred to as “permissive substitutions” (STARR AND THORNTON 2016). They have the potential to make certain mutations accessible that would otherwise remain inaccessible. An obvious

path for evolutionary divergence in msRNAPs would be the incorporation of substitutions with mild effects on fitness but with biochemical properties of increased catalytic activity. These GOF alleles would have properties of suppression of LOF alleles that might otherwise be selected against. Conversely, substitutions with a consistent negative effect, like K1093N and R1100C, may act as "restrictive substitutions", limiting the accessibility of some mutations (STARR AND THORNTON 2016). A limitation of our analyses is that our experiments tested a limited number of backgrounds. In the future, our platform has the capability to determine if the case studies presented here are rarer or the norm in the TL. In summary, our analyses provide a framework for understanding complicated epistatic interactions of substitutions and examples of how fitness landscapes of mutants are changed due to epistasis.

METHODS

Experimental data

Experimental data was collected as described in Duan et al (DUAN *et al.* 2023). Briefly, we synthesized TL mutant libraries including 662 natural TL variants from bacterial, archaeal, and eukaryotic RNA polymerases, 1987 TL haplotypes encompassing every possible substitution combination among seven selected Pol II TL natural variants, 724 TL haplotypes specifically designed for coupling analysis, and 620 TL single mutants serving as control to determine residue interactions. Approximate 15% wild-type *S. cerevisiae* Pol II TL allele of total variants was incorporated into each TL library for accurate quantification. All TL alleles were amplified and transformed into yeast strain CKY283 along with modified RPB1-encoding plasmid to allow construction of complete Rpb1 TL mutants within yeast through gap repair. After transformation, Leu+ colonies were collected, and re-plated into subsequent selection plates. Growth defects and phenotypes of mutants were assessed through amplicon sequencing with Illumina Next-seq (150nt reads). We constructed amplicon sequencing libraries by performing emulsion PCR on the TL region with optimized cycles to preserve the original allele frequencies. Subsequently, we employed two barcodes for multiplexing different samples. Raw sequencing data has been deposited on the NCBI SRA (Sequence Read Archive) database under BioProject PRJNA948661.

Data cleaning and normalization

Each TL variant library was constructed and screened in three biological replicates. Read counts were estimated with a codon-based alignment algorithm [Citation] and the median counts of the three replicates was used in the analysis. Mutant with read counts coefficients of variation > 0.5 in the control condition were excluded from the analysis due to low reproducibility. We calculated fitness scores by comparing allele frequency shifts before and after selections to the shifts of wild type with a formula provided below. To enable direct comparisons, we applied min-max normalization to standardize median growth fitness across all libraries. Residue with fitness equal or smaller to -6.5 is in the severe sick and lethality range and their fitness are normalized to the lethal threshold -6.5. Processed mutant count, fitness and processing codes are available through GitHub (https://github.com/Kaplan-Lab-Pitt/TLs_Screening.git).

$$\text{Fitness (mut)} = \log [f^{\text{mut, sele}} / f^{\text{mut, unsele}}] - \log [f^{\text{WT, sele}} / f^{\text{WT, unsele}}]$$

Determination of functional interactions

Functional interactions were represented by genetic interactions calculated from the log additive model (**Fig. S1**). Primary deviation score of a putative haplotype (abc) = Fitness (abc) – [Fitness (a) + Fitness (b) + Fitness (c)].

We further selected seven Pol II TL alleles and constructed all intermediate substitution combinations. For example, the putative TL haplotype has three different residues compared with wild-type *S. cerevisiae* Pol II TL allele a, b and c, we constructed all combinations of substitutions, which are a, b, c, ab, ac, bc, and abc. And we can calculate the secondary deviation scores for each substitution a, b and c. The secondary deviation score of a are calculated from all haplotypes containing a: Secondary deviation score of a_1 = Fitness (ab) – Fitness (b). Secondary deviation score of a_2 = Fitness (ac) – Fitness (c). Secondary deviation score of a_3= Fitness (abc) – Fitness (bc).

Primary and secondary deviation scores cannot be determined if the expected and observed fitness are both in the ultra-sick/lethal range (both fitness < -6.5). Haplotypes with expected fitness < -6.5 can be separated into two different situations. Firstly, all constituent substitutions are viable, but the sum of the fitness could be smaller than -6.5. This is lethality due to additivity and indicated with a dark gray block in the deviation score heatmaps. Secondly, some of the constituent substitutions or combinations are in lethal range. This lethality is because the haplotype contains at least one single substitution and indicated with a black block in the deviation heatmap.

Functional interactions are determined from the deviation scores. Positive interaction (suppression): deviation score > 1. Additive (No interaction): -1 ≤ deviation score ≤ 1. Negative interaction (synthetic sickness/lethality): deviation score < -1.

Maximum likelihood estimate (σ^2) of a certain substitution is calculated to represent its overall epistatic effect (PARK *et al.* 2022). For a substitution with n non-repetitive secondary deviation scores, its maximum likelihood estimate: $\sigma^2 = \frac{\sum_n (Secondary\ deviation\ score\ of\ a\ substitution)^2}{n}$

Coupling analysis

Coupling analysis was done as described in Russ et al (RUSS *et al.* 2005) and Socolich et al (SOCOLICH *et al.* 2005) with multiple sequence alignment (MSA) of TL sequences. Briefly, three independent TL haplotypes libraries were constructed to study intra-TL co-evolutionary residues. (a). Natural variants library, which is consist of 362 selected natural eukaryotic Pol I, II, and III TL variants. MSA and coupling analysis based on the MSA were done for the selected TL alleles to detect the residue coupling information (**Fig. S2A**). (b). Random scrambling library, where amino acids in the same position of the MSA from (a) were randomly swapped. This swapping does not disturb sequence conservation, because the composition of different amino acids in the position remains unchanged but disrupts residue coupling among different residues. Coupling analysis was done for the random scrambled MSA to confirm disrupted residue coupling (**Fig. S2B**). (c). Monte Carlo scrambling library, where the amino acids in the same position were swapped and then assessed by the Monte Carlo algorithm. If the swapping perturbs residue coupling, we withdraw the swap; if not, we keep the swap. By doing this, the Monte Carlo scrambling library retains both sequence conservation and residue coupling information (**Fig. S2C**). The swapping in both cases breaks the epistasis between TL residues and the Pol II context. TL haplotypes were synthesized based on three types of MSA and then screened for mutant phenotypes through phenotypic system (QIU *et al.* 2016; QIU AND KAPLAN 2019; DUAN *et al.* 2023).

ACKNOWLEDGMENTS

We thank Dr. Anne-Ruxandra Carvunis (U. Pittsburgh) for discussions and advice. We thank Zhizhen Wang and Muyao Lin from the Pitt Statistical Consulting Center for their advice on checking the reproducibility of our data. We acknowledge funding from NIH R01GM097260 for initiation of this project and NIH R35GM144116 for this work. This research was supported in part by the University of Pittsburgh Center for Research Computing RRID:SCR_022735 through the resources provided. Specifically, this work used the HTC cluster, which is supported by NIH award number S10OD028483.

REFERENCES

Bakerlee, C. W., A. N. Nguyen Ba, Y. Shulgina, J. I. Rojas Echenique and M. M. Desai, 2022 Idiosyncratic epistasis leads to global fitness-correlated trends. Science 376**:** 630-635.

Bank, C., R. T. Hietpas, J. D. Jensen and D. N. Bolon, 2015 A systematic survey of an intragenic epistatic landscape. Mol Biol Evol 32**:** 229-238.

Bar-Nahum, G., V. Epshtein, A. E. Ruckenstein, R. Rafikov, A. Mustaev *et al.*, 2005 A ratchet mechanism of transcription elongation and its control. Cell 120**:** 183-193.

Barnes, C. O., M. Calero, I. Malik, B. W. Graham, H. Spahr *et al.*, 2015 Crystal Structure of a Transcribing RNA Polymerase II Complex Reveals a Complete Transcription Bubble. Mol Cell 59**:** 258-269.

Belogurov, G. A., and I. Artsimovitch, 2019 The Mechanisms of Substrate Selection, Catalysis, and Translocation by the Elongating RNA Polymerase. J Mol Biol 431**:** 3975-4006.

Braberg, H., H. Jin, E. A. Moehle, Y. A. Chan, S. Wang *et al.*, 2013 From structure to systems: high-resolution, quantitative genetic analysis of RNA polymerase II. Cell 154**:** 775-788.

Cheung, A. C., and P. Cramer, 2011 Structural basis of RNA polymerase II backtracking, arrest and reactivation. Nature 471**:** 249-253.

Cramer, P., 2002 Multisubunit RNA polymerases. Curr Opin Struct Biol 12**:** 89-97.

Da, L. T., D. Wang and X. Huang, 2012 Dynamics of pyrophosphate ion release and its coupled trigger loop motion from closed to open state in RNA polymerase II. J Am Chem Soc 134**:** 2399-2406.

Dangkulwanich, M., T. Ishibashi, S. Liu, M. L. Kireeva, L. Lubkowska *et al.*, 2013 Complete dissection of transcription elongation reveals slow translocation of RNA polymerase II in a linear ratchet mechanism. Elife 2**:** e00971.

Ding, D., A. G. Green, B. Wang, T. V. Lite, E. N. Weinstein *et al.*, 2022 Co-evolution of interacting proteins through non-contacting and non-specific mutations. Nat Ecol Evol 6**:** 590-603.

Domingo, J., P. Baeza-Centurion and B. Lehner, 2019 The Causes and Consequences of Genetic Interactions (Epistasis). Annu Rev Genomics Hum Genet 20**:** 433-460.

Doud, M. B., O. Ashenberg and J. D. Bloom, 2015 Site-Specific Amino Acid Preferences Are Mostly Conserved in Two Closely Related Protein Homologs. Mol Biol Evol 32**:** 2944-2960.

Duan, B., C. Qiu, S. H. Sze and C. Kaplan, 2023 Widespread epistasis shapes RNA Polymerase II active site function and evolution. bioRxiv.

Fouqueau, T., M. E. Zeller, A. C. Cheung, P. Cramer and M. Thomm, 2013 The RNA polymerase trigger loop functions in all three phases of the transcription cycle. Nucleic Acids Res 41**:** 7048-7059.

Haddox, H. K., A. S. Dingens, S. K. Hilton, J. Overbaugh and J. D. Bloom, 2018 Mapping mutational effects along the evolutionary landscape of HIV envelope. Elife 7.

Hill, W. G., M. E. Goddard and P. M. Visscher, 2008 Data and theory point to mainly additive genetic variance for complex traits. PLoS Genet 4**:** e1000008.

Huang, X., D. Wang, D. R. Weiss, D. A. Bushnell, R. D. Kornberg *et al.*, 2010 RNA polymerase II trigger loop residues stabilize and position the incoming nucleotide triphosphate in transcription. Proc Natl Acad Sci U S A 107**:** 15745-15750.

Johnson, M. S., G. Reddy and M. M. Desai, 2023 Epistasis and evolution: recent advances and an outlook for prediction. BMC Biol 21**:** 120.
Kaplan, C. D., 2010 The architecture of RNA polymerase fidelity. BMC Biol 8**:** 85.
Kaplan, C. D., 2013 Basic mechanisms of RNA polymerase II activity and alteration of gene expression in Saccharomyces cerevisiae. Biochimica Et Biophysica Acta-Gene Regulatory Mechanisms 1829**:** 39-54.
Kaplan, C. D., H. Jin, I. L. Zhang and A. Belyanin, 2012 Dissection of Pol II trigger loop function and Pol II activity-dependent control of start site selection in vivo. PLoS Genet 8**:** e1002627.
Kaplan, C. D., K. M. Larsson and R. D. Kornberg, 2008 The RNA polymerase II trigger loop functions in substrate selection and is directly targeted by alpha-amanitin. Mol Cell 30**:** 547-556.
Kireeva, M. L., Y. A. Nedialkov, G. H. Cremona, Y. A. Purtov, L. Lubkowska *et al.*, 2008 Transient reversal of RNA polymerase II active site closing controls fidelity of transcription elongation. Mol Cell 30**:** 557-566.
Kondrashov, A. S., S. Sunyaev and F. A. Kondrashov, 2002 Dobzhansky-Muller incompatibilities in protein evolution. Proc Natl Acad Sci U S A 99**:** 14878-14883.
Larson, M. H., J. Zhou, C. D. Kaplan, M. Palangat, R. D. Kornberg *et al.*, 2012 Trigger loop dynamics mediate the balance between the transcriptional fidelity and speed of RNA polymerase II. Proc Natl Acad Sci U S A 109**:** 6555-6560.
Lin, X., Y. Liu, S. Liu, X. Zhu, L. Wu *et al.*, 2022 Nested epistasis enhancer networks for robust genome regulation. Science 377**:** 1077-1085.
Liu, B., Y. Zuo and T. A. Steitz, 2016 Structures of E. coli sigmaS-transcription initiation complexes provide new insights into polymerase mechanism. Proc Natl Acad Sci U S A 113**:** 4051-4056.
Lunzer, M., G. B. Golding and A. M. Dean, 2010 Pervasive cryptic epistasis in molecular evolution. PLoS Genet 6**:** e1001162.
Malinen, A. M., M. Turtola, M. Parthiban, L. Vainonen, M. S. Johnson *et al.*, 2012 Active site opening and closure control translocation of multisubunit RNA polymerase. Nucleic Acids Res 40**:** 7442-7451.
Mani, R., R. P. St Onge, J. L. t. Hartman, G. Giaever and F. P. Roth, 2008 Defining genetic interaction. Proc Natl Acad Sci U S A 105**:** 3461-3466.
Mazumder, A., M. Lin, A. N. Kapanidis and R. H. Ebright, 2020 Closing and opening of the RNA polymerase trigger loop. Proc Natl Acad Sci U S A 117**:** 15642-15649.
Melamed, D., D. L. Young, C. E. Gamble, C. R. Miller and S. Fields, 2013 Deep mutational scanning of an RRM domain of the Saccharomyces cerevisiae poly(A)-binding protein. RNA 19**:** 1537-1551.
Metzger, B. P. H., Y. Park, T. N. Starr and J. W. Thornton, 2023 Epistasis facilitates functional evolution in an ancient transcription factor. Elife.
Mosaei, H., and N. Zenkin, 2021 Two distinct pathways of RNA polymerase backtracking determine the requirement for the Trigger Loop during RNA hydrolysis. Nucleic Acids Res 49**:** 8777-8784.
Natarajan, C., N. Inoguchi, R. E. Weber, A. Fago, H. Moriyama *et al.*, 2013 Epistasis among adaptive mutations in deer mouse hemoglobin. Science 340**:** 1324-1327.
Nayak, D., M. Voss, T. Windgassen, R. A. Mooney and R. Landick, 2013 Cys-pair reporters detect a constrained trigger loop in a paused RNA polymerase. Mol Cell 50**:** 882-893.
Olson, C. A., N. C. Wu and R. Sun, 2014 A comprehensive biophysical description of pairwise epistasis throughout an entire protein domain. Curr Biol 24**:** 2643-2651.
Palo, M. Z., J. Zhu, T. V. Mishanina and R. Landick, 2021 Conserved Trigger Loop Histidine of RNA Polymerase II Functions as a Positional Catalyst Primarily through Steric Effects. Biochemistry 60**:** 3323-3336.

Park, Y., B. P. H. Metzger and J. W. Thornton, 2022 Epistatic drift causes gradual decay of predictability in protein evolution. Science 376**:** 823-830.
Phillips, P. C., 1998 The language of gene interaction. Genetics 149**:** 1167-1171.
Phillips, P. C., 2008 Epistasis--the essential role of gene interactions in the structure and evolution of genetic systems. Nat Rev Genet 9**:** 855-867.
Pokusaeva, V. O., D. R. Usmanova, E. V. Putintseva, L. Espinar, K. S. Sarkisyan *et al.*, 2019 An experimental assay of the interactions of amino acids from orthologous sequences shaping a complex fitness landscape. PLoS Genet 15**:** e1008079.
Qiu, C., O. C. Erinne, J. M. Dave, P. Cui, H. Jin *et al.*, 2016 High-Resolution Phenotypic Landscape of the RNA Polymerase II Trigger Loop. PLoS Genet 12**:** e1006321.
Qiu, C., and C. D. Kaplan, 2019 Functional assays for transcription mechanisms in high-throughput. Methods 159-160**:** 115-123.
Reddy, G., and M. M. Desai, 2021 Global epistasis emerges from a generic model of a complex trait. Elife 10.
Russ, W. P., D. M. Lowery, P. Mishra, M. B. Yaffe and R. Ranganathan, 2005 Natural-like function in artificial WW domains. Nature 437**:** 579-583.
Seibold, S. A., B. N. Singh, C. Zhang, M. Kireeva, C. Domecq *et al.*, 2010 Conformational coupling, bridge helix dynamics and active site dehydration in catalysis by RNA polymerase. Biochim Biophys Acta 1799**:** 575-587.
Socolich, M., S. W. Lockless, W. P. Russ, H. Lee, K. H. Gardner *et al.*, 2005 Evolutionary information for specifying a protein fold. Nature 437**:** 512-518.
Starr, T. N., and J. W. Thornton, 2016 Epistasis in protein evolution. Protein Sci 25**:** 1204-1218.
Sydow, J. F., F. Brueckner, A. C. Cheung, G. E. Damsma, S. Dengl *et al.*, 2009 Structural basis of transcription: mismatch-specific fidelity mechanisms and paused RNA polymerase II with frayed RNA. Mol Cell 34**:** 710-721.
Unarta, I. C., E. C. Goonetilleke, D. Wang and X. Huang, 2023 Nucleotide addition and cleavage by RNA polymerase II: Coordination of two catalytic reactions using a single active site. J Biol Chem 299**:** 102844.
Vassylyev, D. G., M. N. Vassylyeva, J. Zhang, M. Palangat, I. Artsimovitch *et al.*, 2007 Structural basis for substrate loading in bacterial RNA polymerase. Nature 448**:** 163-168.
Viktorovskaya, O. V., K. L. Engel, S. L. French, P. Cui, P. J. Vandeventer *et al.*, 2013 Divergent contributions of conserved active site residues to transcription by eukaryotic RNA polymerases I and II. Cell Rep 4**:** 974-984.
Wang, B., A. V. Predeus, Z. F. Burton and M. Feig, 2013 Energetic and structural details of the trigger-loop closing transition in RNA polymerase II. Biophys J 105**:** 767-775.
Wang, D., D. A. Bushnell, X. Huang, K. D. Westover, M. Levitt *et al.*, 2009 Structural basis of transcription: backtracked RNA polymerase II at 3.4 angstrom resolution. Science 324**:** 1203-1206.
Wang, D., D. A. Bushnell, K. D. Westover, C. D. Kaplan and R. D. Kornberg, 2006 Structural basis of transcription: role of the trigger loop in substrate specificity and catalysis. Cell 127**:** 941-954.
Werner, F., and D. Grohmann, 2011 Evolution of multisubunit RNA polymerases in the three domains of life. Nat Rev Microbiol 9**:** 85-98.
Windgassen, T. A., R. A. Mooney, D. Nayak, M. Palangat, J. Zhang *et al.*, 2014 Trigger-helix folding pathway and SI3 mediate catalysis and hairpin-stabilized pausing by Escherichia coli RNA polymerase. Nucleic Acids Res 42**:** 12707-12721.
Xie, X., X. Sun, Y. Wang, B. Lehner and X. Li, 2023 Dominance vs epistasis: the biophysical origins and plasticity of genetic interactions within and between alleles. Nat Commun 14**:** 5551.

Xu, L., K. V. Butler, J. Chong, J. Wengel, E. T. Kool *et al.*, 2014 Dissecting the chemical interactions and substrate structural signatures governing RNA polymerase II trigger loop closure by synthetic nucleic acid analogues. Nucleic Acids Res 42**:** 5863-5870.

Yuzenkova, Y., A. Bochkareva, V. R. Tadigotla, M. Roghanian, S. Zorov *et al.*, 2010 Stepwise mechanism for transcription fidelity. BMC Biol 8**:** 54.

Zhang, J., M. Palangat and R. Landick, 2010 Role of the RNA polymerase trigger loop in catalysis and pausing. Nat Struct Mol Biol 17**:** 99-104.

Figures

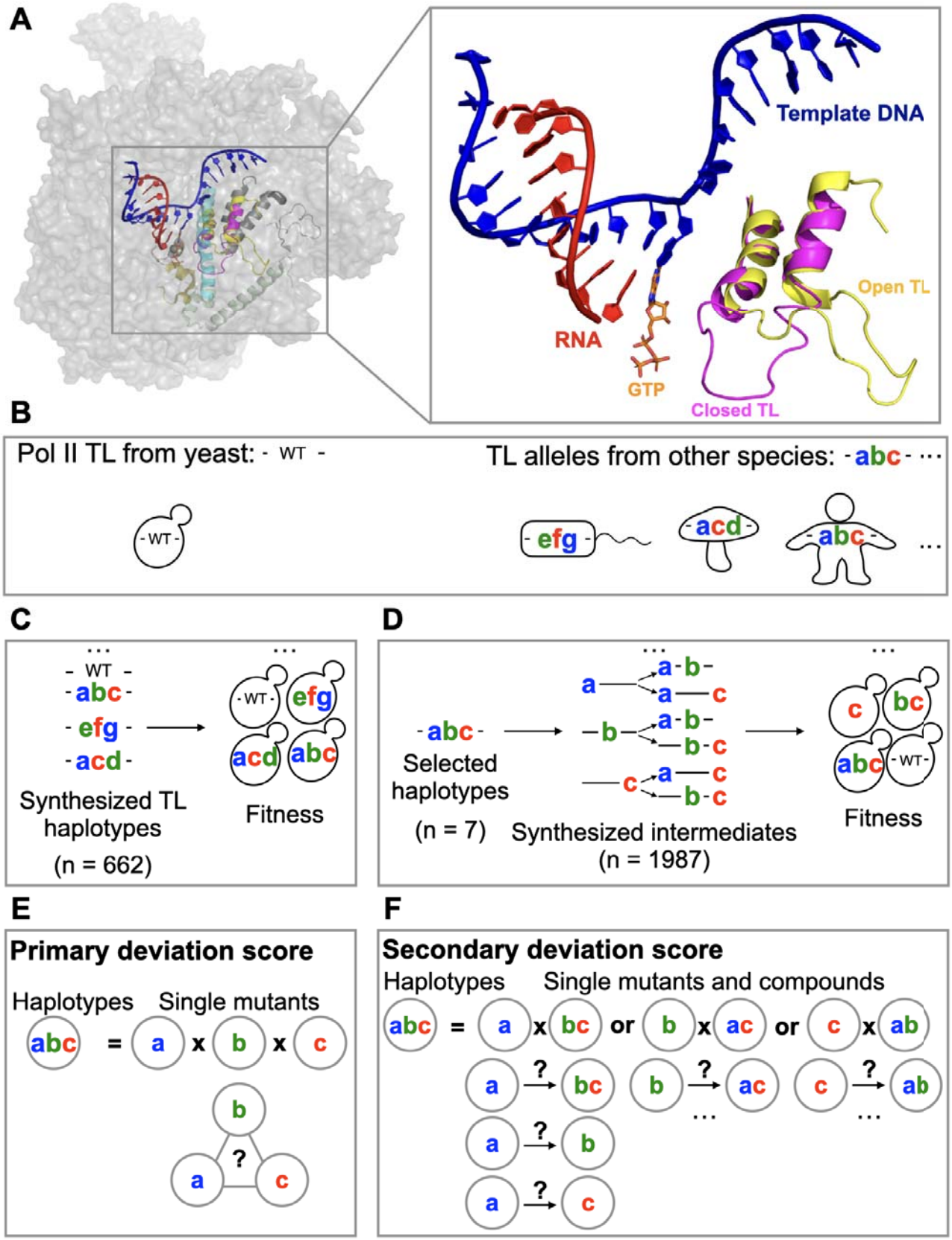
A
Template DNA
Open TL
RNA
GTP
Closed TL
B
Pol II TL from yeast: - WT -
TL alleles from other species: - abc - ···
- WT -
- efg -
- acd -
- abc -
···
C
- WT -
- abc -
- efg -
- acd -
Synthesized TL haplotypes
(n = 662)
- WT -
efg
acd
abc
Fitness
D
- abc -
Selected haplotypes
(n = 7)
a
b
c
a - b -
a — c
a - b -
— b - c
a — c
— b - c
Synthesized intermediates
(n = 1987)
c
bc
abc
- WT -
Fitness
E
Primary deviation score
Haplotypes
Single mutants
abc = a x b x c
b
a
c
?
F
Secondary deviation score
Haplotypes
Single mutants and compounds
abc = a x bc or b x ac or c x ab
a ? bc
b ? ac
c ? ab
a ? b
a ? c

Figure 1. Systematic detection of TL-internal epistasis with natural TL alleles and intermediates. A. The Pol II TL is the key domain balancing transcription speed and fidelity in Pol II active site. Left panel: yeast Pol II structure (PDB: 5C4X). Right panel: The open, catalytic disfavoring (PDB: 5C4X) (BARNES *et al.* 2015) and closed, catalytic favoring (PDB: 2E2H) (WANG *et al.* 2006) conformations of TL in the active site. **B**. We selected 662 TL haplotypes representing TL alleles from bacterial, archaeal and the three conserved eukaryotic msRNAPs to detect TL-internal epistasis. **C**. The selected TL alleles were synthesized and transformed into yeast Pol II to form chimeric Pol II enzymes. Yeast chimeric Pol II enzymes were phenotyped under selective conditions to detect growth defects, which are represented by fitness (see **Methods**). **D**. Seven Pol II TL alleles were selected to construct intermediate haplotypes representing all possible combinations of substitutions of the seven selected alleles. The intermediates were transformed into yeast to measure growth defects as in C. E-F. Analytical scheme of primary deviation score (**E**) and secondary deviation score (**F**). Details are in **Methods**.

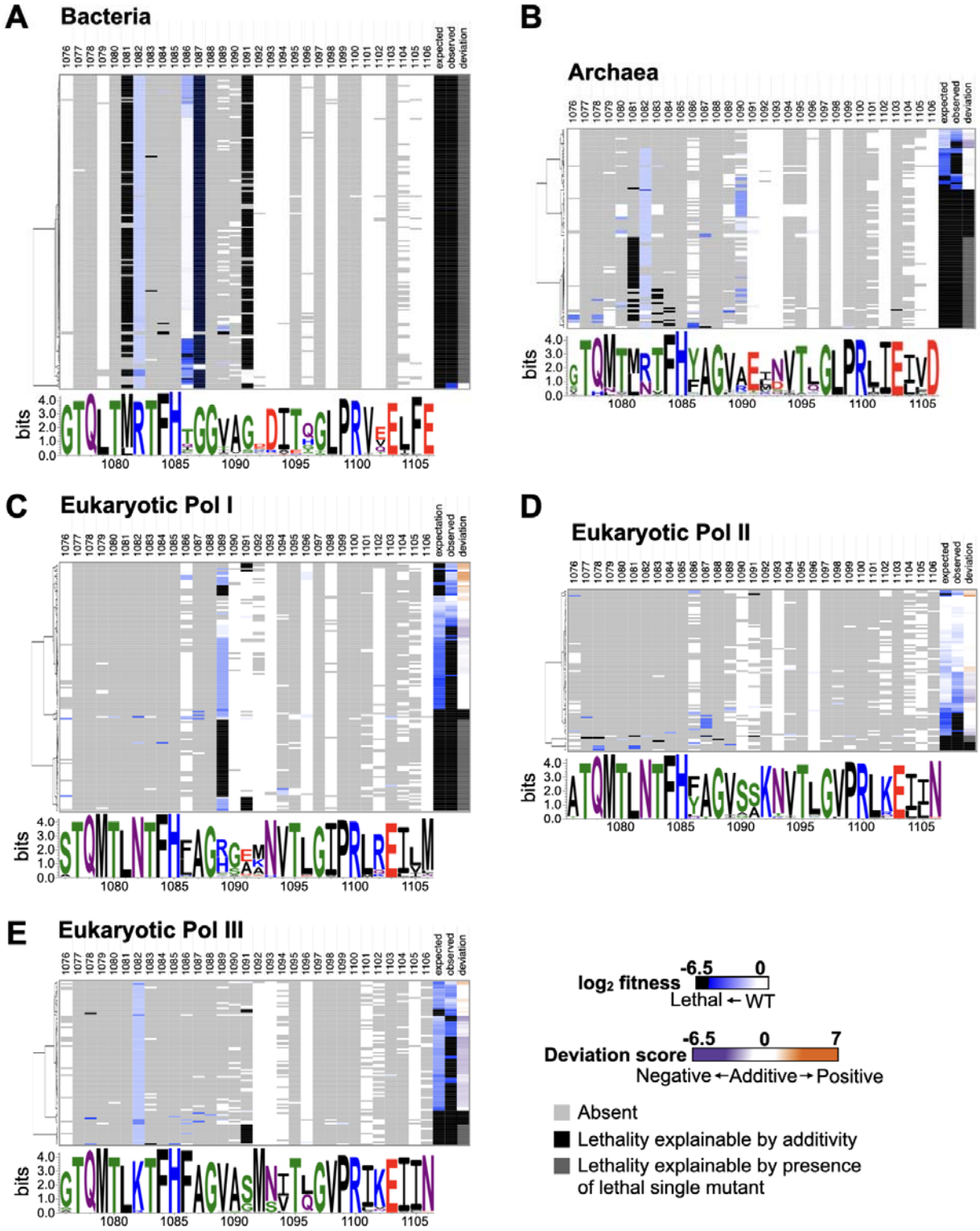
A
Bacteria
B
Archaea
C
Eukaryotic Pol I
D
Eukaryotic Pol II
E
Eukaryotic Pol III
expected
observed
deviation
bits
log2 fitness
-6.5
0
Lethal ← WT
Deviation score
-6.5
0
7
Negative ← Additive → Positive
Absent
Lethality explainable by additivity
Lethality explainable by presence of lethal single mutant

695

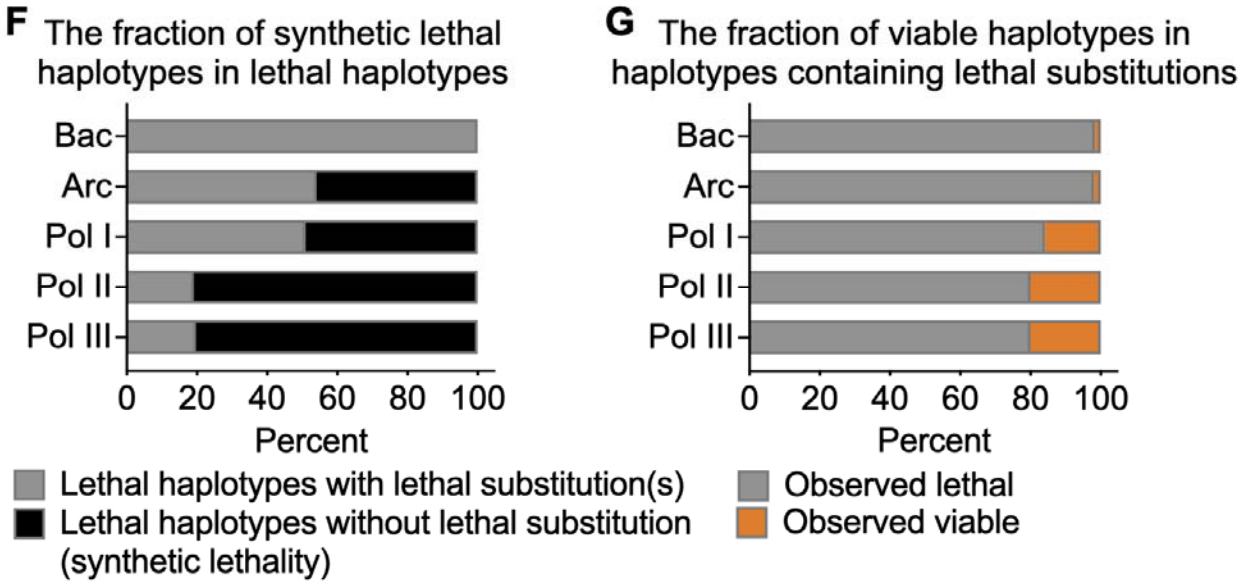

Figure 2. Greater TL-internal epistasis is observed with closer evolutionary distance to eukaryotic Pol II. A-E. Fitness and primary deviation score heatmaps of TL haplotypes from five msRNAP evolutionary groups. The X-axis of each heatmap is the 31 residue positions of the Pol II TL (1076-1106). The Y-axis of each heatmap is the TL haplotypes belonging to each group clustered by hierarchical clustering with Euclidean distance. Each row represents one haplotype with several single substitutions. Light grey blocks in each row represent the residue from the haplotype at the position is the same with yeast Pol II TL residue, in other words, no substitution at the position. Colored blocks represent different residues in the haplotype compared with yeast Pol II TL (substitutions). The color of the block represents growth fitness of the single substitution in the yeast Pol II TL background. Expected fitness of the haplotypes were calculated from the log additive model for individual substitutions. Observed fitness was measured in the screening experiments, and deviation scores were calculated by comparing the observed and expected scores (shown at the right end of each row). Sequence logos were generated with multiple sequence alignment (MSA) of the five groups individually in Weblogo 3.7.12. The labeled numbers of the sequence logo represent yeast Pol II TL residue position (1076-1106). Bacteria n=465. Archaea n=426. Pol I n=605. Pol II n=405. Pol III n=444. **F**. Lethal haplotypes can contain three distinct types of lethality: one attributed to synthetic lethal interactions among substitutions, representing negative interactions that result in lethality beyond expectation, additive lethality expected from combination of individual substitutions, and that arising directly from the presence of an individually lethal single substitution. The calculated ratio specifically reflects the proportion of lethality due to negative interactions and additive lethality within all types of lethal haplotypes. **G**. The ratio of viable haplotypes in haplotypes containing lethal substitutions, representing the ratio of positive interactions (suppression) in TL haplotypes of each group. Haplotypes containing lethal substitutions are expected to be lethal based on the additive model. If haplotypes with lethal substitutions are observed to be viable, it suggests other substitutions suppress the lethal substitution in the haplotypes, implying positive epistasis (suppression). Approximately 20% of examined eukaryotic TL haplotypes containing individual lethal substitutions are viable, whereas only roughly 2% of bacterial and archaeal TL haplotypes are viable, suggesting positive interactions in eukaryotic TLs can buffer negative effects in more closely related TL sequences.

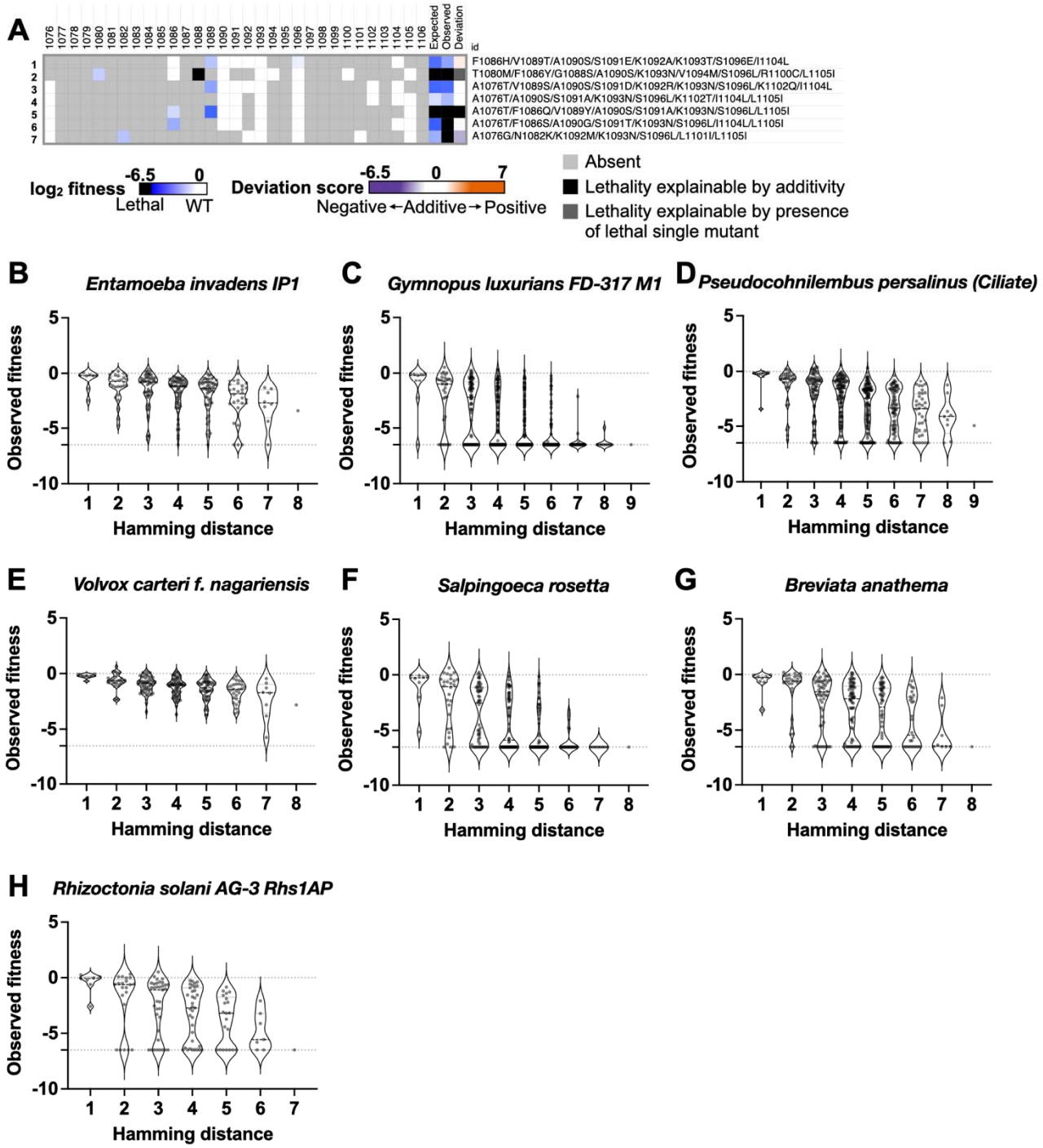

Figure 3. Phenotypes fluctuate with changes in substitution composition within haplotype groups. A. Fitness of constituent single substitutions, and expected and observed fitness of the haplotypes, and deviation score are shown in heatmap for the selected seven haplotypes. The deviations shown in the heatmap are the primary deviation scores calculated by comparing observed fitnesses to expected fitnesses. **B-H**. Distribution of growth fitness across all intermediate substitution combinations categorized by the count of substitutions (hamming distance).

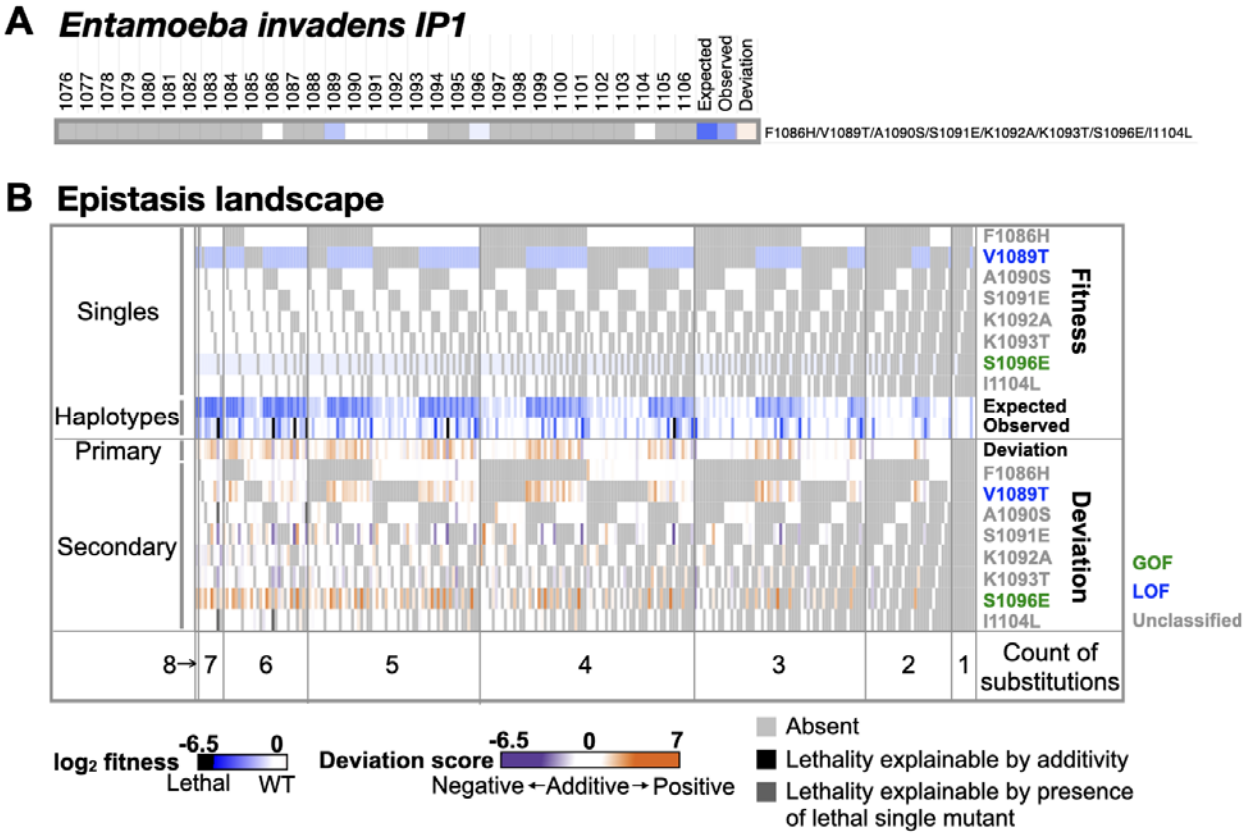

Figure 4. **The epistasis landscape provides a comprehensive view of primary and secondary deviation scores, emphasizing substitutions with notable epistatic effects. A**. Fitness of eight *Entamoeba invadens IP1* TL single substitutions in yeast Pol II background, and the expected and observed fitness and the primary deviation score are shown in the heatmap. **B**. The epistasis landscape of *E. invadens IP1* TL substitutions. The heatmap illustrates the fitness and epistasis of all unique intermediate haplotypes coming from combinations of eight substitutions. Intermediate haplotypes are grouped by counted number of substitutions from 1 to 8. The fitness values are displayed in the upper panel and the epistasis, represented by primary and secondary deviation scores is displayed in the lower panel. The colors of substitution names indicate their phenotypes, GOF is in green, LOF is in blue, unclassified is in grey.

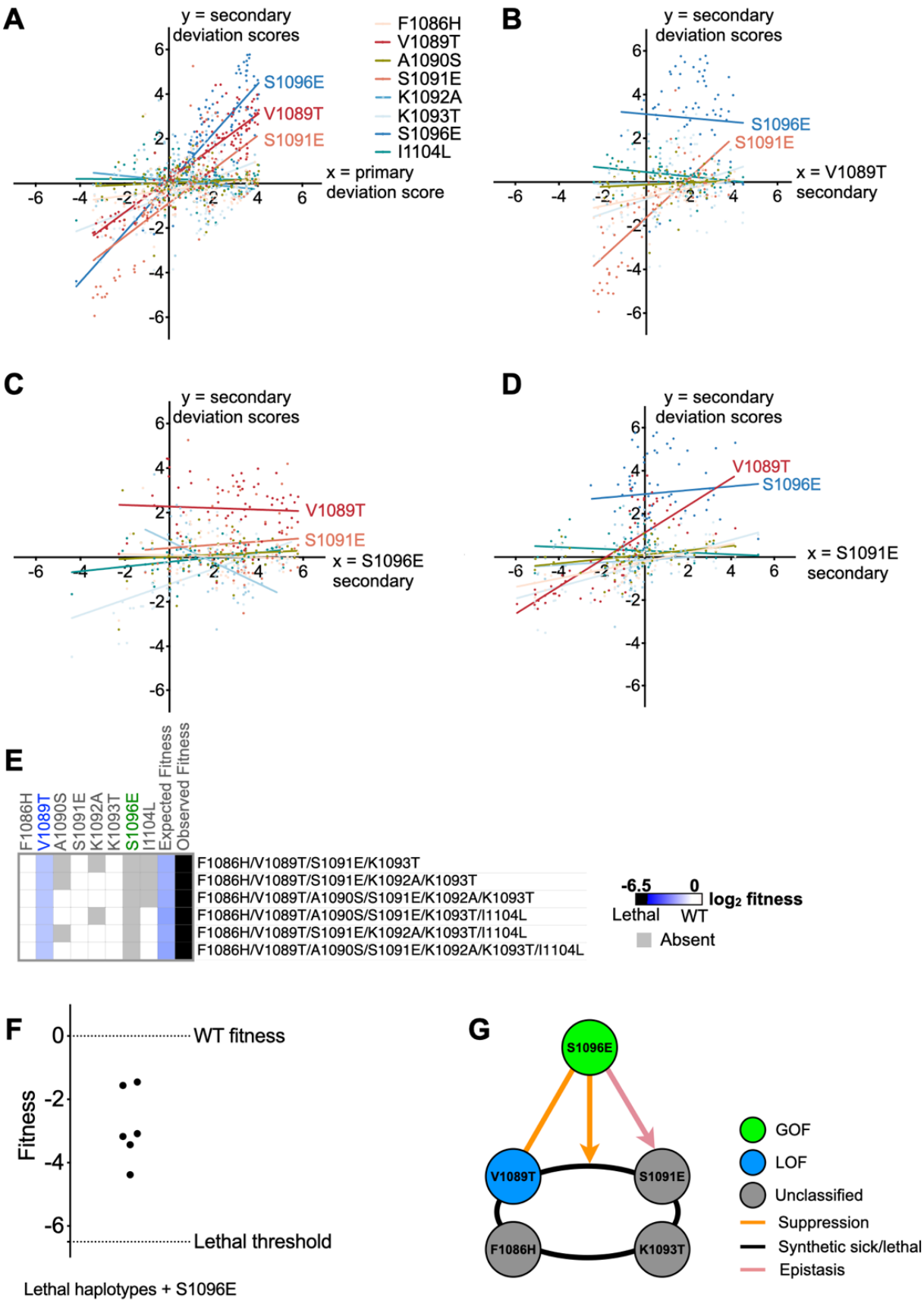
A
y = secondary deviation scores
x = primary deviation score
S1096E
V1089T
S1091E
F1086H
V1089T
A1090S
S1091E
K1092A
K1093T
S1096E
I1104L
B
y = secondary deviation scores
x = V1089T secondary
S1096E
S1091E
C
y = secondary deviation scores
x = S1096E secondary
V1089T
S1091E
D
y = secondary deviation scores
x = S1091E secondary
V1089T
S1096E
E
F1086H
V1089T
A1090S
S1091E
K1092A
K1093T
S1096E
I1104L
Expected Fitness
Observed Fitness
F1086H/V1089T/S1091E/K1093T
F1086H/V1089T/S1091E/K1092A/K1093T
F1086H/V1089T/A1090S/S1091E/K1092A/K1093T
F1086H/V1089T/A1090S/S1091E/K1093T/I1104L
F1086H/V1089T/S1091E/K1092A/K1093T/I1104L
F1086H/V1089T/A1090S/S1091E/K1092A/K1093T/I1104L
-6.5
0
log2 fitness
Lethal
WT
Absent
F
Fitness
WT fitness
Lethal threshold
Lethal haplotypes + S1096E
G
S1096E
V1089T
S1091E
F1086H
K1093T
GOF
LOF
Unclassified
Suppression
Synthetic sick/lethal
Epistasis

746

Figure 5. Correlations between deviation scores reflect specific residue interactions in *E. invadens IP1* TL substitutions. A. Correlations between secondary deviation scores of all eight substitutions (Y-axis) and the primary deviation score (X-axis). Linear regression was applied to each comparison of secondary deviation scores against primary deviation scores to check the correlation. Substitutions with an R^2 value exceeding 0.5 are annotated on the X-Y plot, indicating their substantial impact on primary epistasis of the haplotypes. **B-D**. Correlations between secondary deviations of the other seven substitutions (Y-axis) vs V1089T (**B**), S1096E (**C**), S1091E (**D**) on the X-axes respectively. **E**. The fitness landscape of intermediate combinations with fitnesses in the ultra-sick/lethal range. Their observed fitness levels are in the lethal range as indicated with black blocks in the heatmap while the expected fitness scores calculated from the additive model is in viable range (light blue blocks), indicating potential negative interactions. The fitness scores of the constituent single mutants within lethal haplotypes are shown in the heatmap. F1086H, V1089T, S1091E, and K1093T are present in each lethal haplotype while S1096E is absent. Names of substitutions are colored based on their phenotypes. GOF: green. LOF: blue. No obvious phenotype: grey. **F**. The fitness of all ultra-sick to lethal haplotypes with S1096E incorporated is no longer in the ultra-sick/lethal range. **G**. Scheme of specific residue interactions within substitutions of *E. invadens IP1* TL.

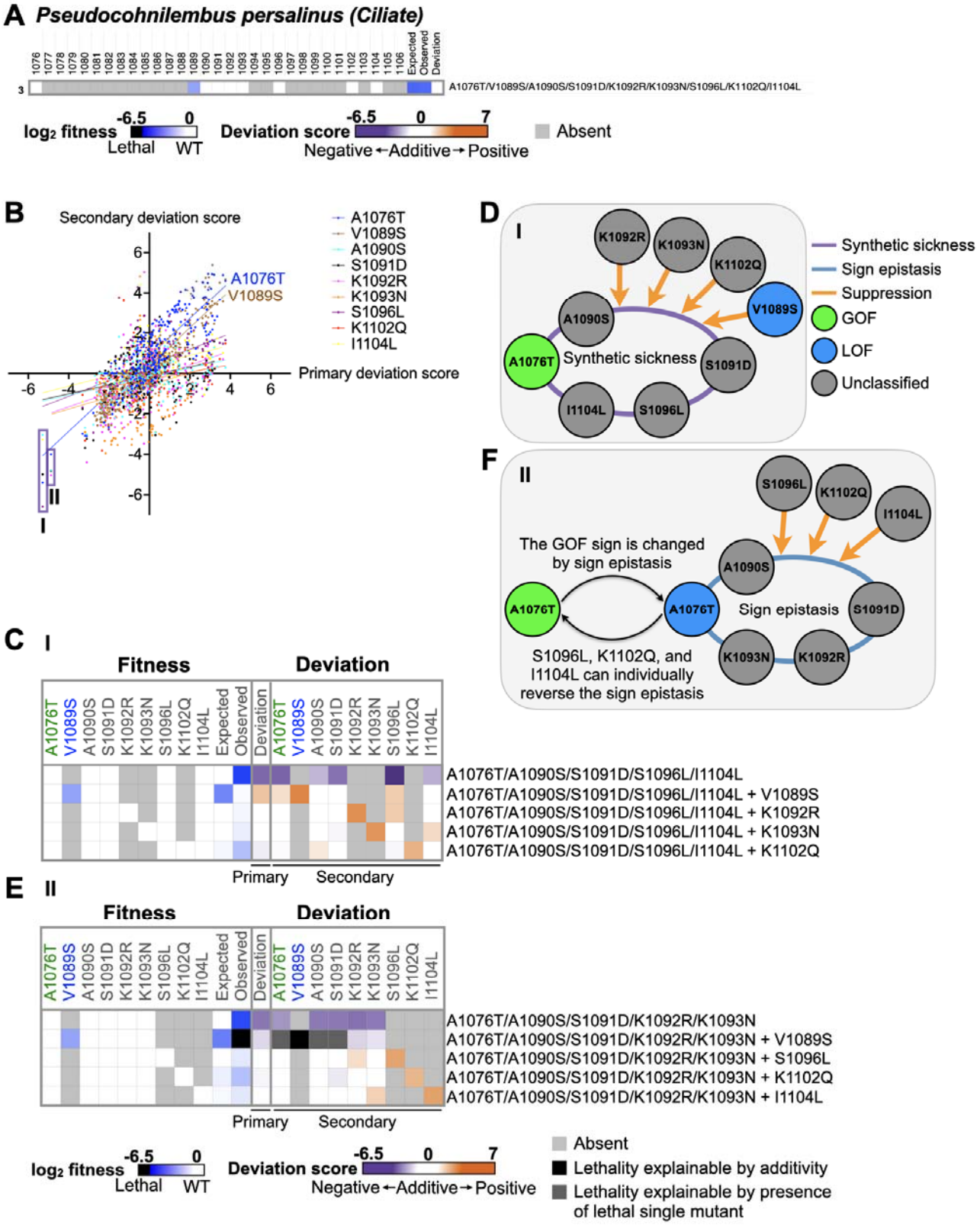
A Pseudocohnilembus persalinus (Ciliate)
A1076T/V1089S/A1090S/S1091D/K1092R/K1093N/S1096L/K1102Q/I1104L
log2 fitness -6.5 0 Lethal WT
Deviation score -6.5 0 7 Negative ← Additive → Positive
Absent
B
Secondary deviation score
Primary deviation score
A1076T
V1089S
A1090S
S1091D
K1092R
K1093N
S1096L
K1102Q
I1104L
D
Synthetic sickness
Sign epistasis
Suppression
GOF
LOF
Unclassified
F
The GOF sign is changed by sign epistasis
Sign epistasis
S1096L, K1102Q, and I1104L can individually reverse the sign epistasis
C
Fitness
Deviation
Expected
Observed
Deviation
A1076T/A1090S/S1091D/S1096L/I1104L
A1076T/A1090S/S1091D/S1096L/I1104L + V1089S
A1076T/A1090S/S1091D/S1096L/I1104L + K1092R
A1076T/A1090S/S1091D/S1096L/I1104L + K1093N
A1076T/A1090S/S1091D/S1096L/I1104L + K1102Q
Primary
Secondary
E
A1076T/A1090S/S1091D/K1092R/K1093N
A1076T/A1090S/S1091D/K1092R/K1093N + V1089S
A1076T/A1090S/S1091D/K1092R/K1093N + S1096L
A1076T/A1090S/S1091D/K1092R/K1093N + K1102Q
A1076T/A1090S/S1091D/K1092R/K1093N + I1104L
Absent
Lethality explainable by additivity
Lethality explainable by presence of lethal single mutant

Figure 6. Intricate higher-order epistasis observed in substitutions of *P. persalinus (Ciliate)* TL haplotype. A. The heatmap displays the fitness of nine single substitutions in *P. persalinus (Ciliate)* TL in the yeast Pol II background, along with the epistasis between them represented by the primary deviation score. **B**. Similar to Fig. 5A, we checked correlations between secondary deviation scores (Y-axis) to the primary deviation score (X-axis) to identify substitutions with substantial impact on primary deviation scores. Simple linear regression was applied to each comparison. Substitutions with $R^2 > 0.5$ are annotated in the plot. **C**. The fitness and deviation scores of substitution combinations related to group I are shown in the heatmap. Names of substitutions are colored based on their phenotypes. GOF: green. LOF: blue. No obvious phenotype (unclassified): grey. Each line shows the fitness and deviation scores of substitutions in a certain combination. Left, the fitness of individual substitutions, and the expected and observed fitness. Right, the primary deviations calculated by comparing observed and expected fitness and the secondary deviation scores of each constituent substitution. A1076T/A1090S/S1091D/S1096L/I1104L is in the first line. Its observed fitness is smaller than expected and when compared, resulting in a negative primary deviation score, representing a negative interaction. The secondary deviation scores of each constituent substitutions are all negative, indicating each of them showing negative interactions when adding to corresponding compounds. The following four lines represent the four combinations where V1089S, K1092R, K1093N, and K1102Q are incorporated into A1076T/A1090S/S1091D/S1096L/I1104L respectively. All observed fitness of combinations is healthier than A1076T/A1090S/S1091D/S1096L/I1104L, and the secondary deviation scores of V1089S, K1092R, K1093N and K1102Q are all positive, implying positive effect (suppression) on each combination respectively. **D**. Scheme illustrating the substitution interaction network observed in C. **E**. Similar to C, the fitness and deviation scores of combinations related with group II are shown in the heatmap. The first row shows the fitness and deviation scores detected within the combination A1076T/A1090S/S1091D/K1092R/K1093N. The following rows displays the corresponding fitness and deviation scores when the other four substitutions are incorporated. Notably, the effect of V1089S on A1076T/A1090S/S1091D/K1092R/K1093N cannot be determined because the observed fitness of the combination (V1089S + A1076T/A1090S/S1091D/K1092R/K1093N) is in the ultra-sick/lethal range, and its expected fitness calculated from the log additive model is also in the lethal range. However, V1089S and the compounds are sick but viable. The expected lethality is due to additivity. In this case, the secondary deviation of V1089S cannot be calculated and is represented by a black block in the heatmap. Moreover, the effect of A1076T on V1089S/A1090S/S1091D/K1092R/K1093N cannot be determined because the observed fitness falls within the lethal range. The expected fitness of (A1076T + V1089S/A1090S/S1091D/K1092R/K1093N) is also in the lethal range due to the presence of the lethal compound V1089S/A1090S/S1091D/K1092R/K1093N. The expected lethality of the combination is because it contains a lethal component. The secondary deviation score of A1076T cannot be determined either and is indicated by a dark gray block in the heatmap. **F**. Scheme representing the substitution interaction networks observed in E.

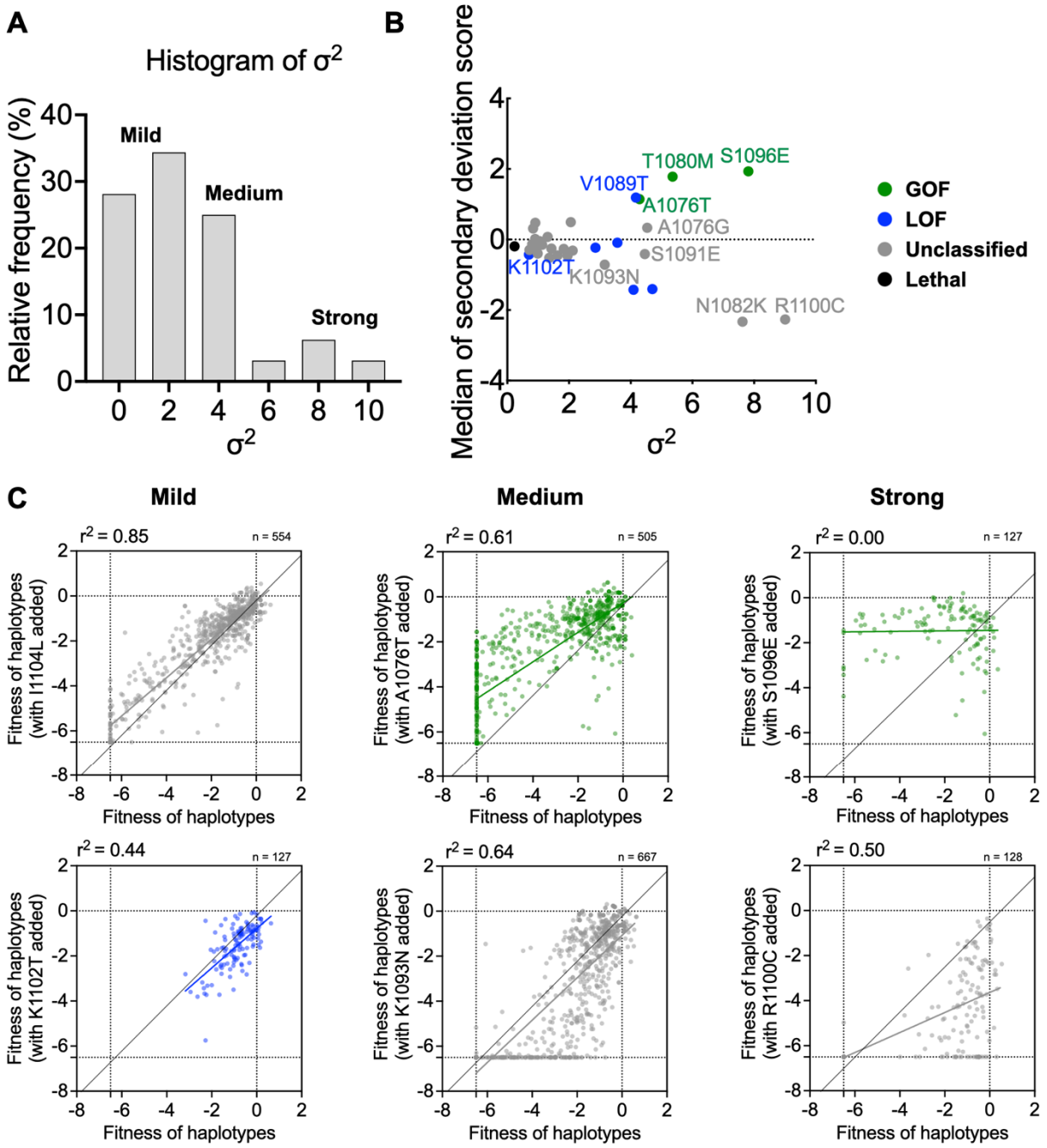

Figure 7. Different classes of epistatic effects. A. Histogram of mutants' epistatic effects, represented by their respective maximum likelihood estimate (σ^2) of secondary deviation scores. Higher epistatic effect indicates greater impact of a certain substitution. **B**. Medians of secondary deviation scores of substitutions were plotted against their corresponding σ^2. Substitutions are colored based on their phenotypes. **C**. Comparing epistatic effects of mutants in each category. Each scatter plot shows the measured fitness of haplotypes without (X-axis) versus with (Y-axis) a substitution incorporated. The colors of the plots represent the mutants' phenotypes. The colored line marks the simple linear regression of the spots, representing the observed epistatic effect of the substitution. R^2 values of the regressions are labeled in the plots. The black line indicates the additive (non-epistatic) expectation.

Primary deviation score	= Fitness(abc) - [Fitness(a) + Fitness(b) + Fitness(c)]
a VS **bc**	Secondary deviation score $(a)^1$ = Fitness(abc) - [Fitness(a) + Fitness(bc)]
a VS **b**	Secondary deviation score $(a)^2$ = Fitness(ab) - [Fitness(a) + Fitness(b)]
a VS **c**	Secondary deviation score $(a)^3$ = Fitness(ac) - [Fitness(a) + Fitness(c)]
b VS **ac**	Secondary deviation score $(b)^1$ = Fitness(abc) - [Fitness(b) + Fitness(ac)]
	…
c VS **ab**	Secondary deviation score $(c)^1$ = Fitness(abc) - [Fitness(c) + Fitness(ab)]
	…

Deviation score > 1, suppression, positive epistasis

Deviation score ≈ 0, additive, independent

Deviation score < -1, synthetic sick or lethal, negative epistasis

Figure S1. Detection of higher-order interactions by primary and secondary deviation scores. For a pseudo haplotype “abc”. The primary deviation score is calculated by comparing the observed fitness of the haplotype to the log additive of constituent substitutions’ fitness. The secondary deviation score of “a” in “abc” represents the epistatic effect of “a” on “bc” and is calculated by comparing the observed fitness score of “abc” to the additive of fitness scores of “a” and “bc”. The secondary deviation score of “a” in “ab” represents the epistatic effect of “a”on “b”. It is calculated by comparing the observed fitness score of “ab” to the additive of fitness scores of “a” and “b”. If the deviation score ≈ 0, it indicates the constituent substitutions are independent and there is no interaction among them. If the deviation score > 1, it represents positive epistasis (suppression) among the constituent substitutions. If the deviation score < -1, it represents negative epistasis (synthetic sickness or lethality) among the constituent substitutions.

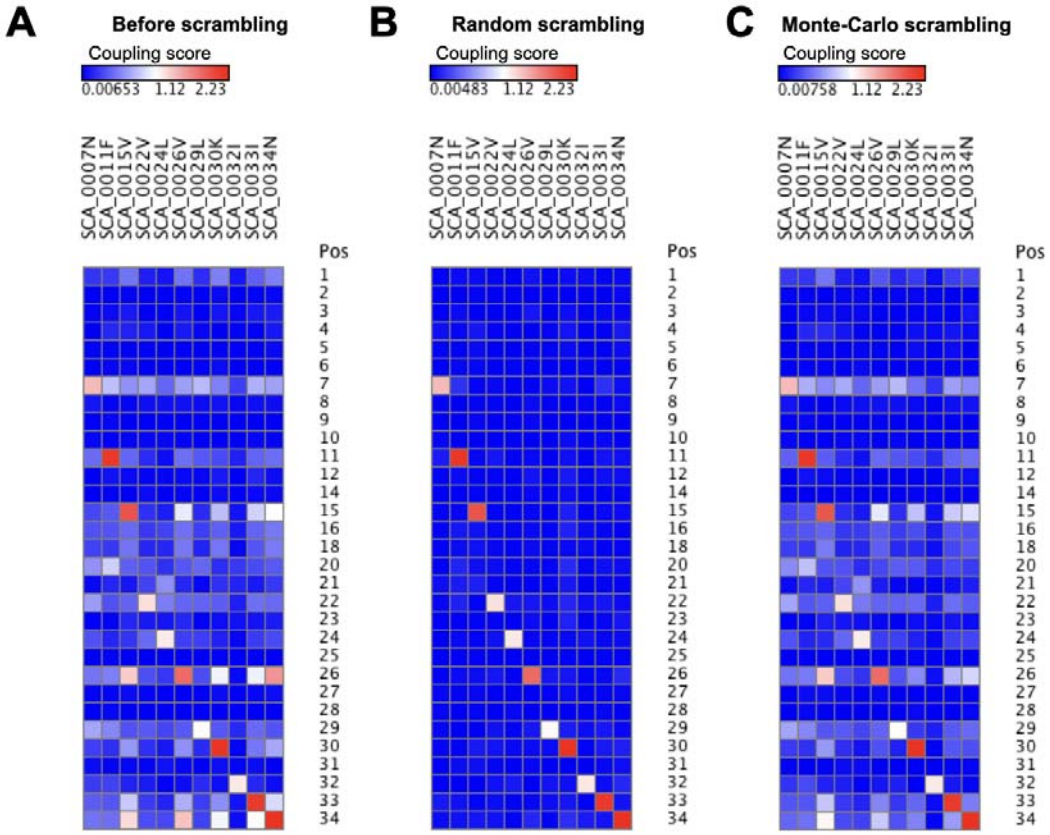
A
Before scrambling
Coupling score
0.00653 1.12 2.23
B
Random scrambling
Coupling score
0.00483 1.12 2.23
C
Monte-Carlo scrambling
Coupling score
0.00758 1.12 2.23
SCA_0007N
SCA_0011F
SCA_0015V
SCA_0022V
SCA_0024L
SCA_0026V
SCA_0029L
SCA_0030K
SCA_0032I
SCA_0033I
SCA_0034N
Pos

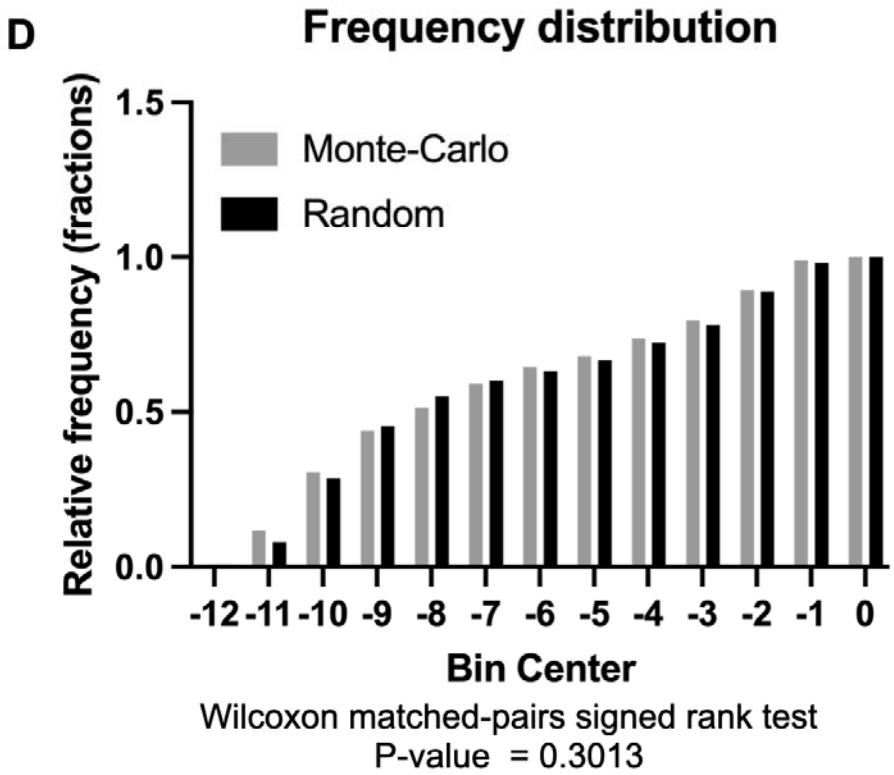
D
Frequency distribution
Monte-Carlo
Random
Relative frequency (fractions)
1.5
1.0
0.5
0.0
-12 -11 -10 -9 -8 -7 -6 -5 -4 -3 -2 -1 0
Bin Center
Wilcoxon matched-pairs signed rank test
P-value = 0.3013

832

Figure S2. Design of mutant libraries to assess TL-internal residue coupling. A. Residue coupling heatmaps of natural TL variants. Statistical coupling analysis of TL multiple sequence alignment including 362 selected natural eukaryotic Pol I, II, and III TL alleles. **B-C**. Heatmaps of coupled residues in Random scrambling and Monte Carlo scrambled haplotypes. The random scrambling disrupted coupled residues in selected TL variants (**B**) while the Monte Carlo scrambling haplotypes reserved coupled residues (**C**). **D**. Cumulative fitness frequency distribution of the Random scrambling and Monte Carlo scrambling haplotypes. The Wilcoxon matched-pairs signed rank test was used to assess the significance of the fitness distribution difference between Monte Carlo scrambling and Random scrambling haplotypes. The P-value of 0.3013 is not significant.

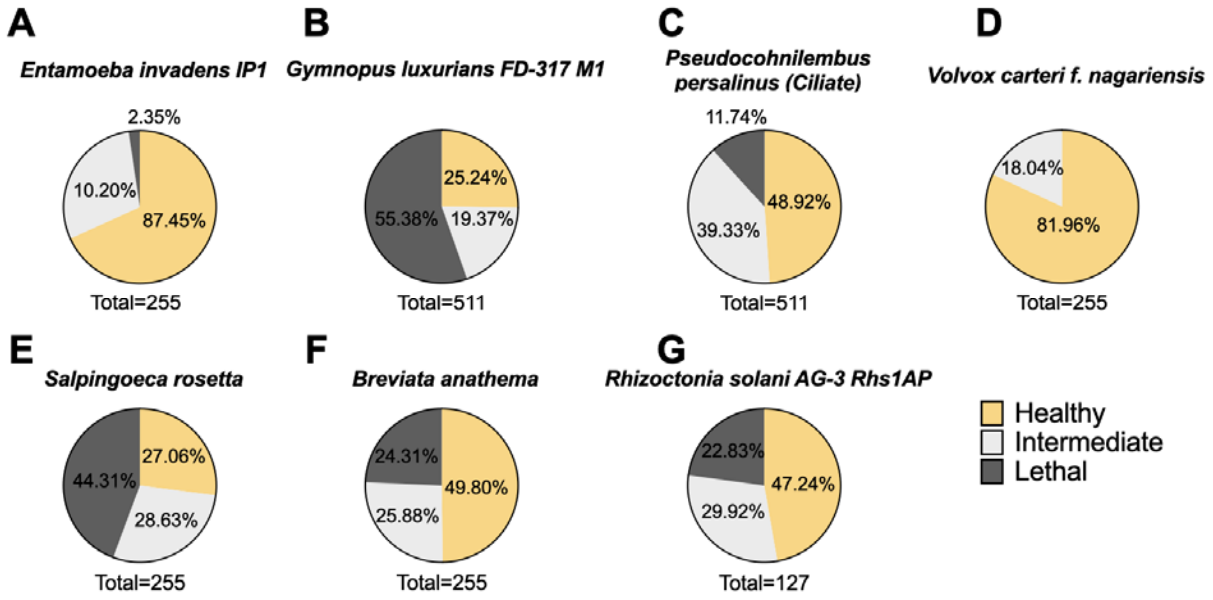

Figure S3. The percentage of fitness categories of all intermediate combinations within each haplotype (A-G). Healthy: Fitness > -2. Intermediate: -6.5 < Fitness ≤ -2. Lethal: Fitness ≤ -6.5.

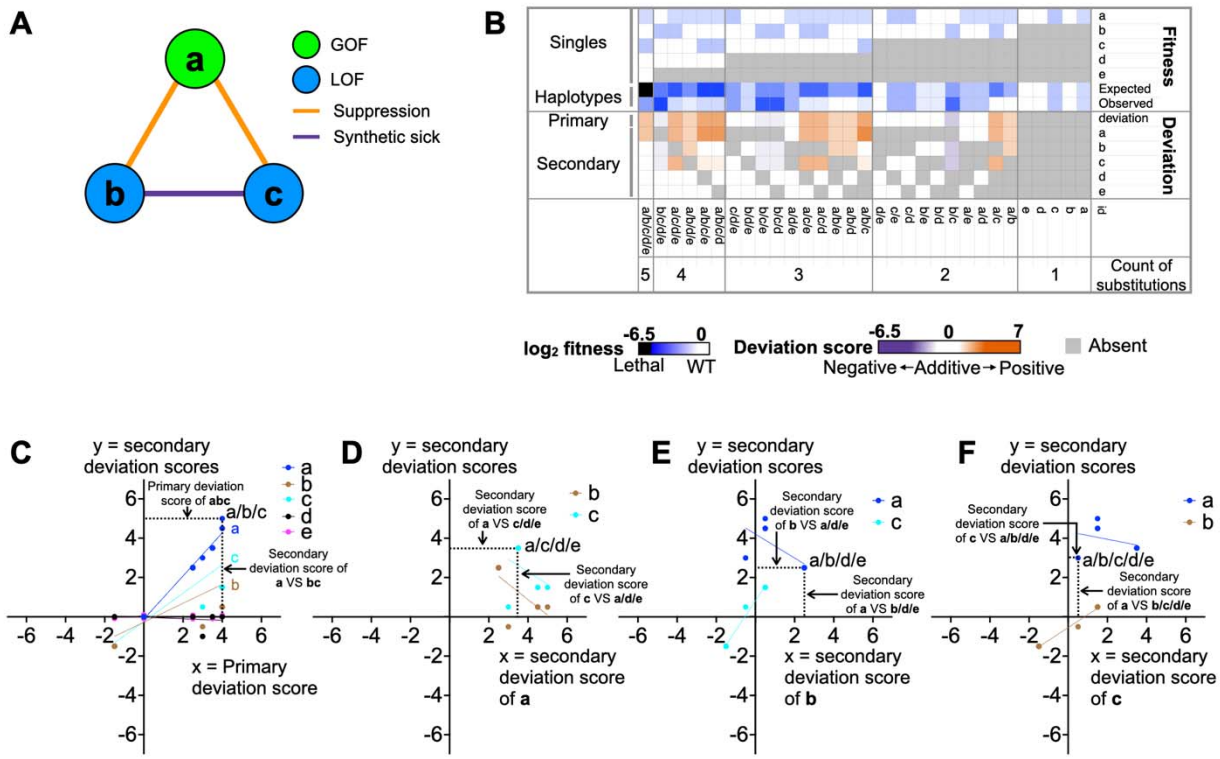

Figure S4. Example primary and secondary deviation scores for a simplified, simulated TL haplotype "abcde". A. Simulated interactions among substitutions "a", "b", and "c". We set the single mutant "a" as a GOF mutant, "b" and "c" as LOF mutants, while "e" and "f" have no effects. We also set suppression between GOF and LOF combinations ("ab" and "ac"), and synthetic sickness between LOF and LOF combinations ("bc"). **B**. The epistasis interaction landscape of simplified TL haplotype "abcde", illustrating the observed and expected fitness of all single substitutions and all intermediate haplotypes, as well as primary and secondary deviation scores in the simulation. **C**. Correlations between secondary deviation scores of all five single substitutions (Y-axis) to the corresponding primary deviation scores (X-axis). To measure the correlation, linear regression was applied for secondary deviation scores of "a", "b", "c", "d", "e" to the corresponding primary deviations scores, respectively. Single substitutions with strong correlations ($R^2 > 0.5$) were labeled in the plot. Three substitutions with phenotypes show strong correlations in the simulation, "a", "b", and "c". **D-F**. The correlation between secondary deviation scores of the four substitutions (Y-axis) vs "a" (**D**), "b" (**E**), "c" (**F**) on X-axis respectively. To read the plot, with **D** as an example, each cyan spot represents an intermediate combination containing both "a" and "c". The labeled spot represents a specific combination "a/c/d/e". Its coordinate value in X-axis represents the secondary deviation score of "a" to "c/d/e". Its coordinate value in Y-axis represents the secondary deviation score of "c" to "a/d/e". We did a linear regression for all the cyan spots to represent the correlation between the secondary deviation scores of "c" to "a". This correlation helps illustrate the potential interaction between "c" and "a". The secondary deviation scores of "c" are all positive when "a" is present, meaning "c" constantly shows positive secondary score when "a" is present, indicating potential suppression of "c" to "a".

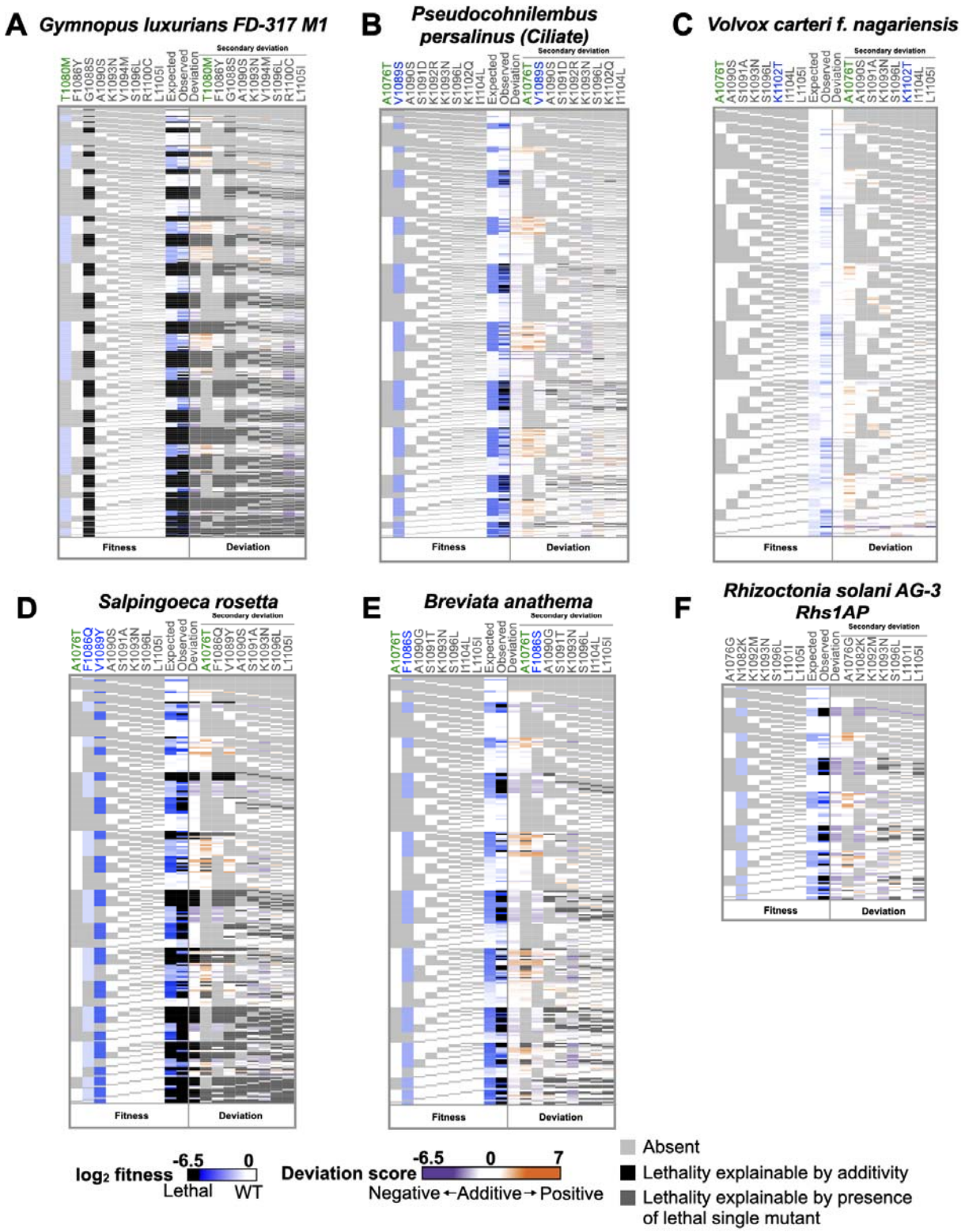

Figure S5. The epistasis landscapes of selected haplotypes. The fitness and epistasis of all unique intermediate haplotypes from combinations of substitutions within each haplotype (**A-F**). The colors of mutants' names represent mutants' phenotypes. GOF is in green, LOF is in green, non-classified mutants is in grey.

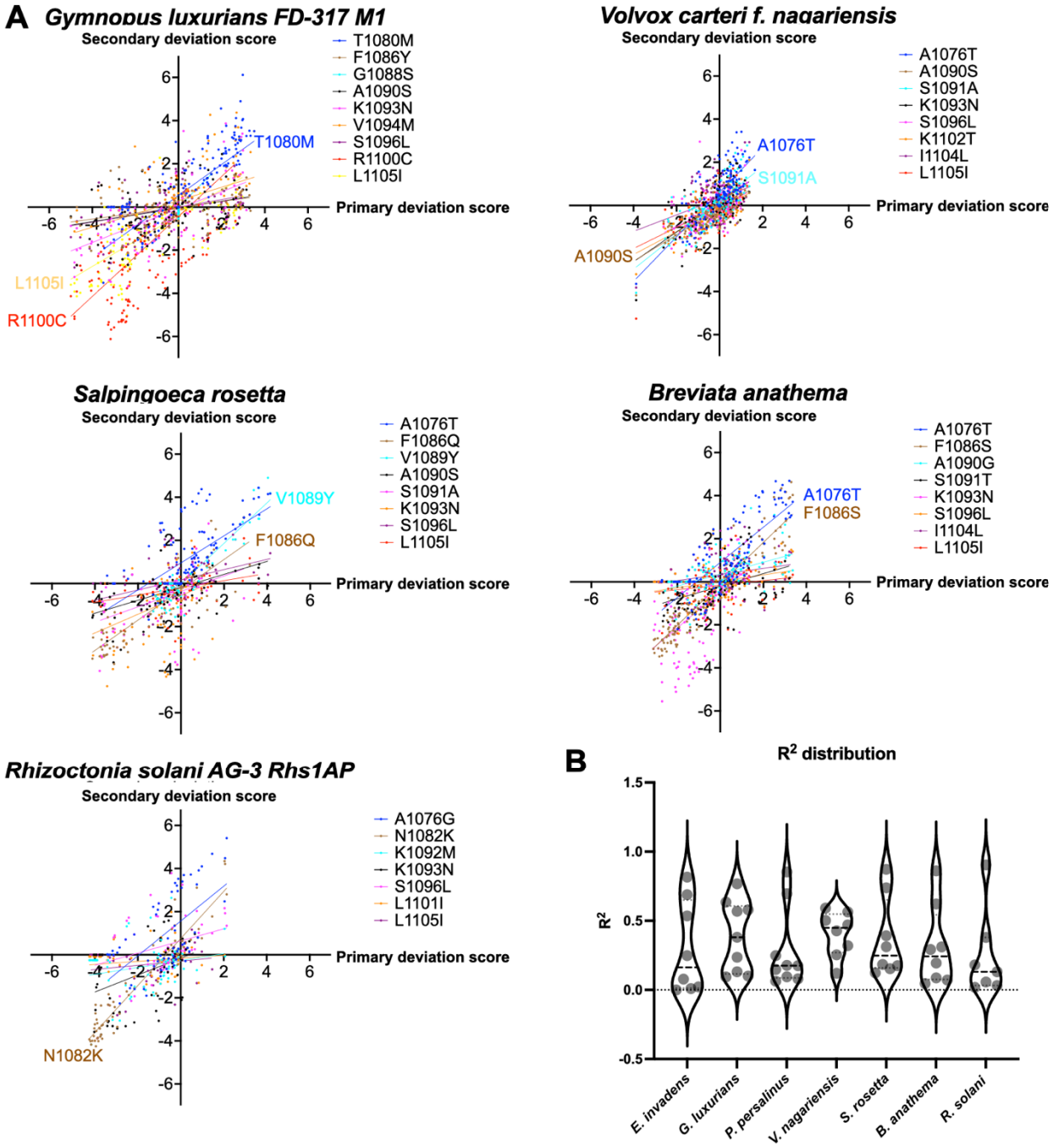

Figure S6. The epistasis within haplotypes is driven by several specific substitutions. A. The correlations between secondary deviation scores of all substitutions (Y-axis) and the primary deviation score (X-axis) for each selected haplotype. Linear regression was applied to each comparison of secondary to primary deviation scores. Substitutions with R^2 value exceeding 0.5 are annotated on the X-Y plot, indicating their substantial impact on primary epistasis of the haplotypes. **B**. Distributions of R^2 of all selected TL haplotypes.

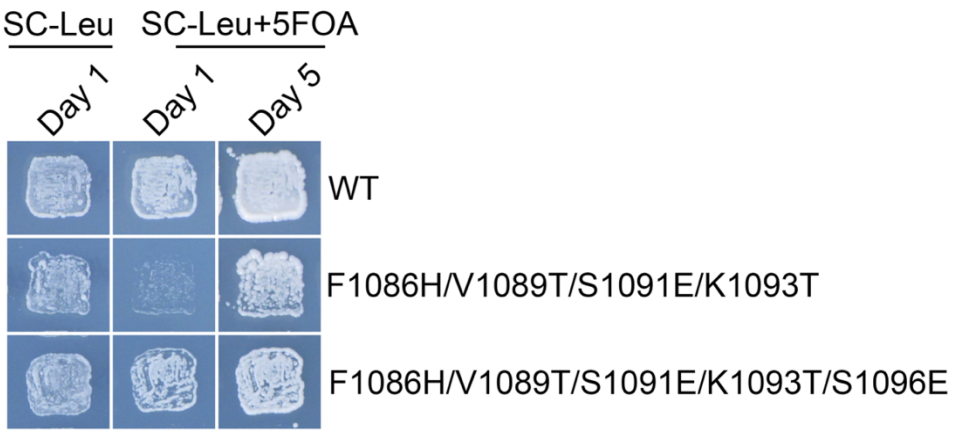

Figure S7. Verification of S1096E suppression on a synthetic sick intermediate haplotype F1086H/V1089T/S1091E/K1093T using patch assay. Sequences of both haplotypes were synthesized and verified by sequencing. Growth on SC-Leu+5FOA indicates the growth defects of the haplotypes. SC-Leu is the control condition where WT *RPB1* is present.

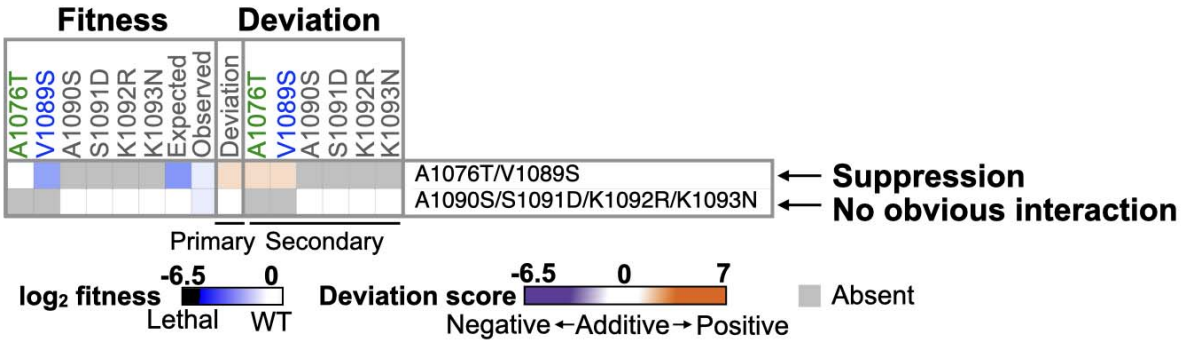

Figure S8. Heatmap displaying fitness and deviation scores in A1076T/V1089S and A1090S/S1091D/K1092R/K1093N. Positive deviation scores in A1076T/V1089S indicate suppression, and no deviations (primary and secondary deviation scores are around zero) indicate no interactions within A1090S/S1091D/K1092R/K1093N.

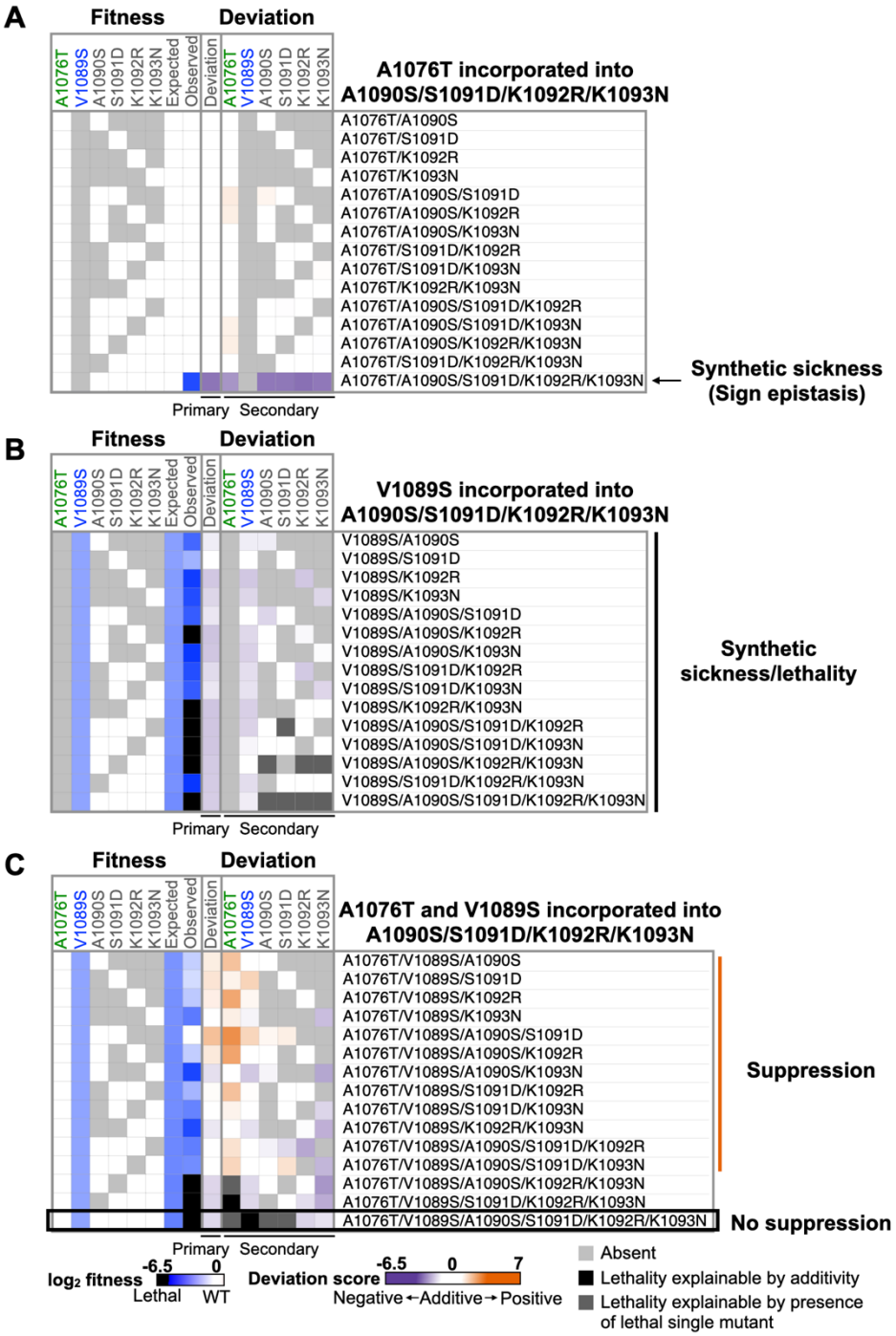

Figure S9. A1076T showed sign epistasis with A1090S/S1091D/K1092R/K1093N. A. Heatmap displays fitness and deviation scores for A1076T in all single substitutions and combinations with A1090S, S1091D, K1092R, K1093N, suggesting A1076T only showed negative interaction with A1090S/S1091D/K1092R/K1093N. **B**. Heatmap shows fitness and deviation scores for V1089S in all single substitutions and combinations with A1090S, S1091D, K1092R, K1093N. V1089S showed negative interactions with almost all of them. **C**. Heatmap shows fitness and deviation scores for A1076T and V1089S in all single substitutions and combinations with A1090S, S1091D, K1092R, K1093N. Positive interactions were observed in most combinations.

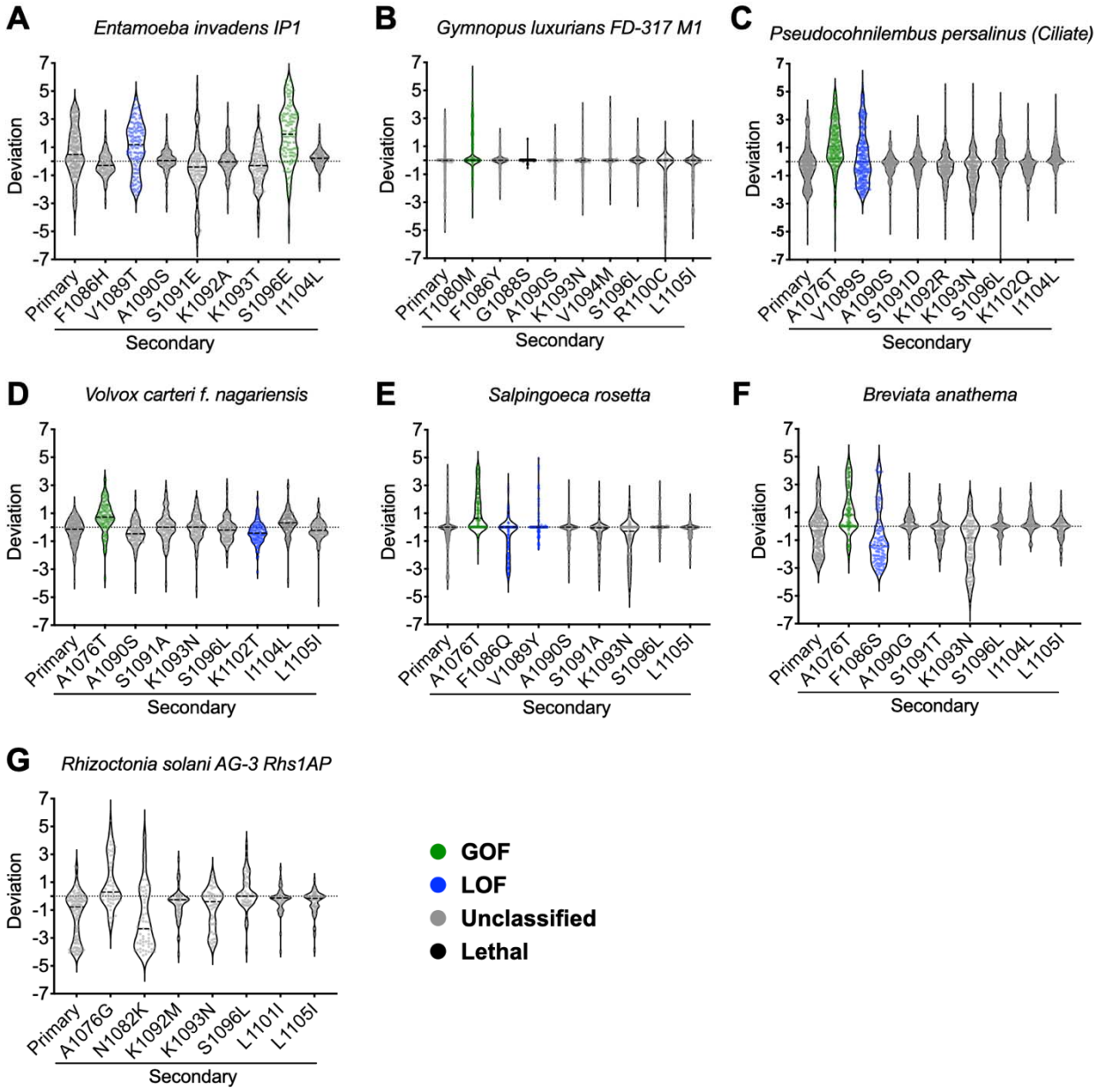

Figure S10. The distributions of primary and secondary deviation scores within each selected haplotype (**A-G**)**.** Colors of spots represent phenotypes of substitutions.

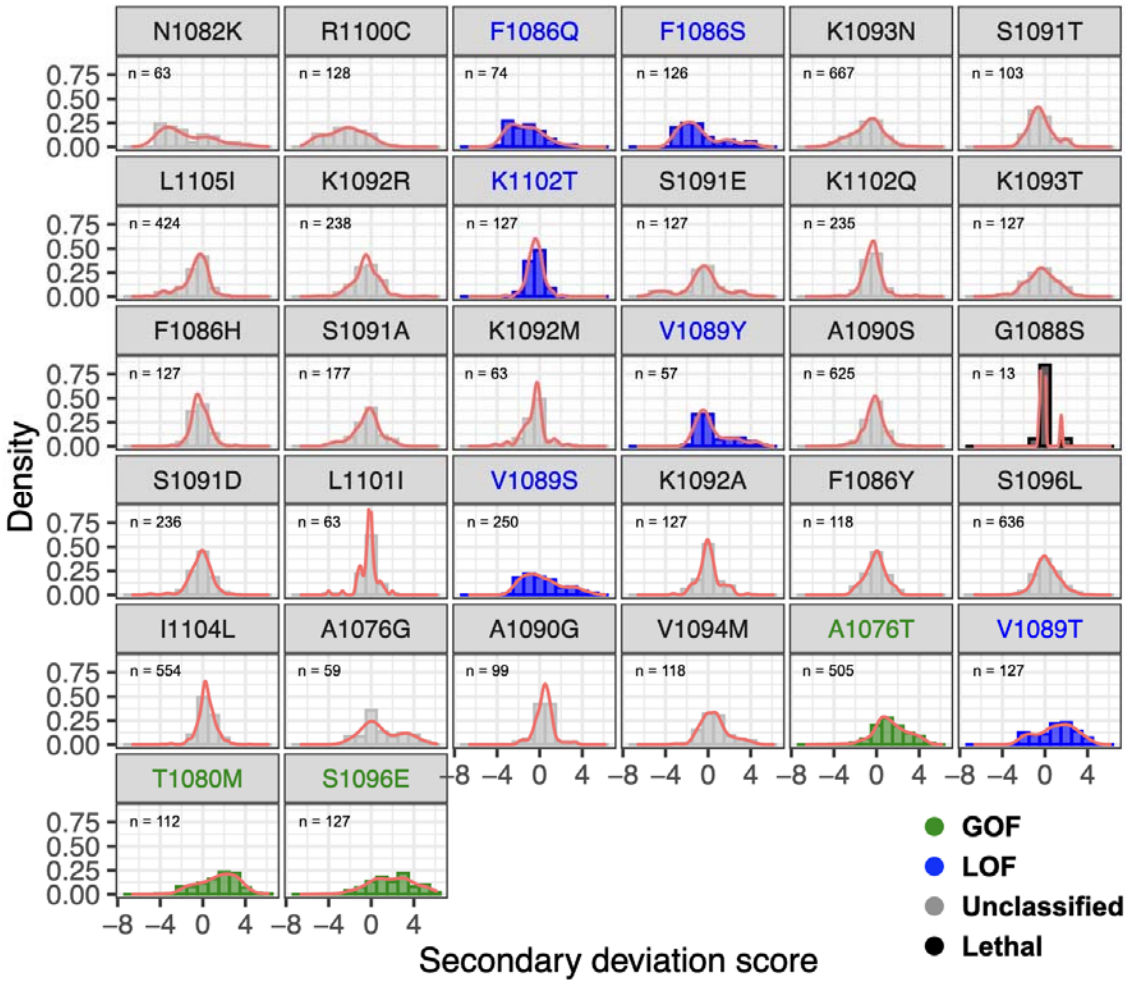

Figure S11. The density plots of secondary deviation scores of each substitution. We made density plots to display the distribution of secondary deviation scores for each substitution. The density plots were calculated of substitutions from nonrepetitive intermediate combinations across all haplotypes. The count of nonrepetitive intermediate combinations containing the substitution is shown in the upper left of each plot.

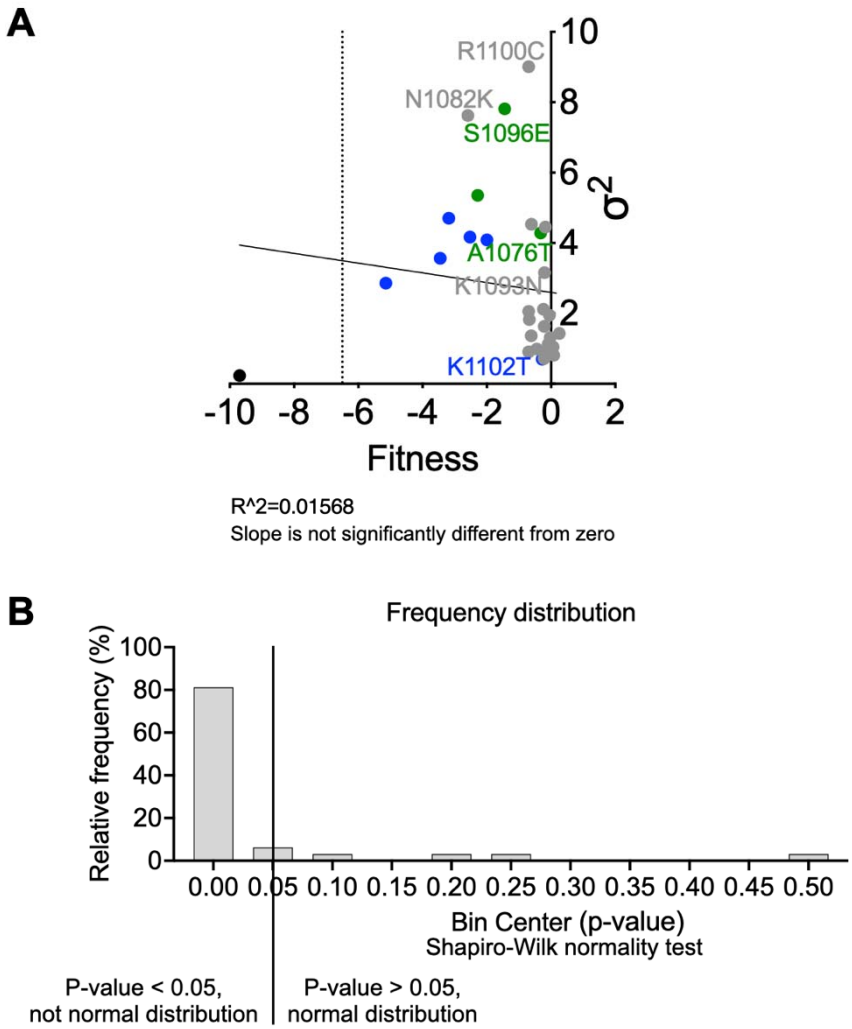

Figure S12. Slight but not significant negative correlation between σ^2 and fitness of substitutions. A. The correlation between the maximum likelihood estimate (σ^2) and the fitness of each substitution. Simple linear regression was applied (Y = -0.1384*X + 2.600, R^2 = 0.01568). The slope is not significantly different from zero (P = 0.5101). **B**. The histogram of p-values from normality test. The density plots of secondary deviation scores have been tested whether they follow normal distribution by Shapiro-Wilk normality test. The null hypothesis of the test is the distribution follows normal distribution. Substitutions with P-value > 0.05 suggest their distributions are normal and P-value < 0.05 indicate their distributions do not follow normal distribution. ~80% of substitutions do not follow normal distribution.